APPLICATION OF AUTOMATED BALANCING METHODS FOR AN ATTITUDE CONTROL TEST PLATFORM WITH NON-ORTHOGONAL MASSES

THESIS

Keith A. Hudson, Capt, USAF

AFIT-ENY-MS-18-J-076

DEPARTMENT OF THE AIR FORCE
AIR UNIVERSITY

AIR FORCE INSTITUTE OF TECHNOLOGY

Wright-Patterson Air Force Base, Ohio

The views expressed in this thesis are those of the author and do not reflect the official policy or position of the United States Air Force, the United States Department of Defense or the United States Government. This is an academic work and should not be used to imply or infer actual mission capability or limitations.

AFIT-ENY-MS-18-J-076

APPLICATION OF AUTOMATED BALANCING METHODS FOR AN ATTITUDE CONTROL TEST PLATFORM WITH NON-ORTHOGONAL MASSES

THESIS

Presented to the Faculty

Department of Aeronautics and Astronautics

Graduate School of Engineering and Management

Air Force Institute of Technology

Air University

Air Education and Training Command

in Partial Fulfillment of the Requirements for the

Degree of Master of Science in Astronautical Engineering

Keith A. Hudson, BS

Capt, USAF

June 2018

AFIT-ENY-MS-18-J-076

APPLICATION OF AUTOMATED BALANCING METHODS FOR AN ATTITUDE CONTROL TEST PLATFORM WITH NON-ORTHOGONAL MASSES

Keith A. Hudson, BS
Capt, USAF

Approved:

Andrew J. Lingenfelter, PhD (Co-Chairman)	Date
Joshuah A. Hess, PhD (Co-Chairman)	Date
Kirk W. Johnson, PhD (Member)	Date

AFIT-ENY-MS-18-J-076

Abstract

Ground-based spacecraft simulators provide an accessible and necessary platform for testing and evaluating control systems. The Attitude Control System Proving Ground (ACSPG) at the Air Force Research Laboratory (AFRL) allows for testing and verifying the performance of attitude control systems. Through the use of an air bearing, the frictionless environment is replicated, but gravitational torques are still prevalent. Gravitational torques distort and negatively affect the sustained performance of simulators, limiting experimentation time.

Cost effective validation efforts require decreasing current set up times and increasing current experimentation times. The distance between the center of rotation (COR) and the center of mass (COM) of the simulator results in unwanted gravitational torques, causing a tilting and unbalanced platform. Developing an automated system to precisely co-locate the COR and the COM will reduce said torques.

This research demonstrates two control techniques to improve the current system balancing procedures. The first method is a non-linear adaptive control and is validated with three primary scenarios, demonstrating an ability to reduce angular velocities to zero. Through tuning, the control algorithm balances the platform according to design constraints. The second method estimates the offset between the COM and COR utilizing a least squares estimation method. The second method is validated with two tests of varying lengths and is able to estimate the offset within 0.5%.

To my family:

"You miss 100% of the shots you don't take.-Wayne Gretzky"-Michael Scott

Acknowledgements

My journey at AFIT was not that of a single individual, and there are many people I must recognize.

First, thank you to my family for your unwavering support and providing energy, hugs, clean laundry, and motivation.

Thank you to my classmates for your unending encouragement and aid.

Thank you to Capt Joshuah Hess for your thorough assistance and guidance.

Finally, I would like to thank my research advisor, Capt Lingenfelter who has kept me on track and guided me through my thesis project every step of the way.

Keith A. Hudson

Table of Contents

Page

List of Figures

Figure Page

List of Tables

List of Acronyms

U.S. United States

AFRL Air Force Research Laboratory

ACSPG Attitude Control System Proving Ground

ADCS attitude determination and control systems

AFIT Air Force Institute of Technology

ASTREX Advanced Space Structure Technology Research Experiments

CMG control moment gyroscopes

COM center of mass

COR center of rotation

DOF degrees of freedom

DMBS dynamic mass balance system

EKF extended Kalman filter

GNC guidance, navigation, and control

HIT Harbin Institute of Technology

IMUs inertial measurement units

KF Kalman filter

MATLAB Matrix Laboratory

MOI moment of inertia

NPS Naval Postgraduate School

ODE ordinary differential equation

RWs reaction wheels

SMBS static mass balancing system

UKF unscented Kalman filter

List of Symbols and Nomenclature

$\dagger$	Moore-Penrose pseduoinverse
$\frac{d\vec{r}_i}{dt}$	First derivative of the position Vector, also velocity
$\vec{F}$	Force
$\vec{g}^{\,b}$	Gravity vector in the body frame
$[\vec{g}^{\,b}\times]$	Skew-symmetric matrix notation
$\vec{g}^{\,i}$	Gravity vector in the inertial frame
$\vec{H}$	Angular momentum
$\dot{\vec{H}}$	First derivative of angular momentum, also torque or moment
$\mathbb{I}$	Identity matrix
$\bar{J}$	Moment of inertia tensor
k_p	Positive scalar tuning constant
$\vec{L}$	Moment or torque, also the first derivative of angular momentum
m_i	i^{th} mass
m_p	Mass of each sliding mass
M	Mass of the entire ACSPG
M_{str}	Mass of the ACSPG not including the sliding masses
P_p	Projection matrix
q	Quaternion
R_i^b	Rotation matrix from the inertial to body reference frame
$\vec{r}_i$	Position vector of the i^{th} mass relative to the COR
$\vec{r}_{str}$	Position vector of the COM of the ACSPG not including sliding masses relative to
$\vec{r}_{off}$	Position vector of the COM relative to the COR
$\hat{\vec{r}}_{off}$	Estimated position vector of the COM relative to the COR
$\tilde{\vec{r}}_{off}$	Error between $\hat{\vec{r}}_{off}$ and $\vec{r}_{off}$
t	Time

$V(\bar{x})$	Scalar Lyapunov function
$\bar{x}^*$	Equilibrium value for use in Lyapunov stability
δ r	Change in position
δ t	Change in time
Θ	Rotation angle about the y-axis
κ	simplifying term representing -$m_{str}[\vec{g}^{\,b}\times]$
$\vec{\tau}_r$	Control Torque for the Nonlinear Adaptive Control
Φ	Rotation angle about the x-axis
Ψ	Rotation angle about the z-axis
$\vec{\omega}$	Angular Velocity
$\vec{\omega}_g$	Angular velocity parallel to the gravity vector
$\vec{\omega}_p$	Angular velocity perpendicular to the gravity vector
$\dot{\vec{\omega}}$	First derivative of angular velocity, also angular acceleration

APPLICATION OF AUTOMATED BALANCING METHODS
FOR AN ATTITUDE CONTROL TEST PLATFORM
WITH NON-ORTHOGONAL MASSES

I. Introduction

1.1 Motivation

The United States (U.S.) AFRL operates the ACSPG. The ACSPG is a spacecraft simulator consisting of a large air bearing and a multi-level test platform, with a mass of approximately 1,375 kg. It is used for a multitude of projects in testing attitude determination and control systems (ADCS) in an environment with minimal external disturbances.

It is important to state early the term "simulator" is a misnomer. It is, however, the conventional term utilized widely throughout the literature discussing similar test platforms. "Emulator" is more accurate as precisely replicating the space environment is not possible with physical models. However, using platforms such as the ACSPG and similar experimental designs, allows for modeling and applying the effects of the space environment. To maintain consistency with the industry, this paper uses the term simulator [2].

The ACSPG is capable of 3-axis movement with ± 30, 30, and 360 degrees of motion in the roll, pitch, and yaw directions respectively. Rotating on a large hemispherical air bearing, the ACSPG uses a variety of computers and sensors for gathering experimental data and controlling the motion of the ACSPG. Compressed air thrusters and control moment gyroscopes (CMG) actuate the attitude of the

ACSPG. AFRL has worked on perfecting its test platform, utilizing hardware designed and developed in conjunction with the Air Force Institute of Technology (AFIT).

This chapter discusses the significance of spacecraft simulators and their applications. First, a historical review of spacecraft simulators is presented. Second, an overview of the proposed system is provided. Third, the problems and motivations for this this research are outlined. Finally, this chapter provides an overview of the thesis.

1.2 Background

Regular use of spacecraft test platforms over the past 60 years allows for lower costs and lower risks when designing attitude control and decision making systems, often referred to as guidance, navigation, and control (GNC) systems) [1]. As with any test platform, the accuracy of the results depends on the ability of the platform to accurately replicate the real-world environment, or in this case, the space environment. The greatest shortcoming of a ground based test platform is the effect of gravitational torques not encountered in space.

When the ACSPG is modified by either adding or subtracting equipment, the COM no longer coincides with the COR. Gravitational torques disturb the system causing the system to no longer exist in a state of equilibrium. Minimizing the distance between the simulator's COM and COR minimizes those torques. Balancing the system realigns the COM and COR, eliminating the gravitational torques. The ACSPG requires a lengthy manual balancing procedure of adding incremented masses one at a time as a static mass balancing system (SMBS). Lasting several hours, this mass balancing procedure still does not fully align the COM and COR.

1.3 Spacecraft Simulator Review

Ideally, researchers could test every new control system in the most realistic environment possible, in this case space. Unfortunately such testing is cost prohibitive. However, to reduce the cost and minimize the risks involved, tests are conducted on Earth in a controlled environment [1]. After systems are refined, they are moved to the space environment, with the hopes of replicating their performance. Models tested in a laboratory setting experience forces not encountered in space, such as increased torques due to gravity. To simulate a weightless environment, astronauts practice their techniques underwater [3]. This is not feasible for testing attitude control systems. Thusly, they are tested on spacecraft simulators.

Spacecraft simulators tend to fall into two categories. The two categories are planar and rotational systems. Planar systems allow for translation to simulate rendezvous maneuvers, while spherical systems ideally allow for unconstrained rotational movement. Many governmental, academic, and commercial facilities have opperated simulators for over five decades. Utilizing compressed air flowing between two spherical surfaces, a nearly frictionless surface is generated. The U.S. government at AFRL and the U.S. Naval Research Laboratory operate two of the largest spherical air-bearing simulators and use the simulators to research various attitude control topics.

1.4 Problem Statement

As was previously stated, the ACSPG requires a lengthy balancing procedure before any testing and experimentation begins or whenever the payload is modified. Requiring between two to four hours of balancing each time the payload is altered, regularly modifying the payload quickly becomes a costly effort. The imprecise

initial balancing leaves the ACSPG subject to environmental torques such as those induced by gravity. As the COM drifts from the COR, efforts are necessary to reduce the generated torques [4].

The internal torques of the spacecraft cause rotation, requiring a reaction in the opposite direction. Utilizing rotors and gimbals, CMGs generate torques on flywheels, increasing the angular momentum. CMGs can offset the torques experienced by a spacecraft [5]. During the operation of the ACSPG, it is able to maintain balance using CMGs as the system detects the current torques and provides torques to counteract the environmental torques. Unfortunately, the CMGs reach their operational limitations and "saturate" within short periods of time, often less than 30 seconds.

The ACSPG destabilizes too quickly for AFRL's experimental purposes as the initial balance point is close, but not exact. The lengthy system reset times and short experimentation times are problems requiring a solution to improve the capabilities of the system. As such, the need exists for a procedure to balance the platform more quickly and accurately. This research presents a unique procedure for implementing a dynamic mass balance system (DMBS), which will prevent the system from destabilizing and improve the accuracy and duration of performed tests.

While appearing rigid, the steel test platform on the ACSPG still flexes. The COM is continually changing as the platform rotates, especially in tilted or off-axis maneuvers. The desire exists to eventually implement a solution to account for and offset the changes due to the flexing of the platform.

1.5 Similar Research

Previous research regarding automatic balancing of satellite simulators focuses on much smaller systems. One common method of balancing smaller simulators is

through the utilization of CMGs [6]. AFRL utilizes CMGs to counteract torques and maintain the balance. However, they easily saturate and are not a sustainable solution. The Naval Postgraduate School (NPS) identified further limitations of using reaction wheels and CMGs, namely the requirement for a consistent amount of weight and volume. To eliminate these limitations, NPS developed their own DMBS [7]. AFRL evaluations have determined the dynamics and controls required for smaller satellites do not scale well to larger systems. It is imperative to consider and capture the complexities of the larger ACSPG structure.

In designing a mass balance system, the configuration of the masses is critical to developing the needed dynamics equations. Researchers at the NPS have employed orthogonal configurations, aligning the masses with the Cartesian coordinate system [7]. Researchers at the Harbin Institute of Technology (HIT) in China have developed a non-orthogonal structure [1]. AFRL has modeled and simulated different designs, ultimately deciding on a non-orthogonal configuration comprised of five masses on linear actuators, three horizontally aligned with the center of the air bearing, offset from each other at 120 degrees, and two coupled linear actuators positioned vertically.

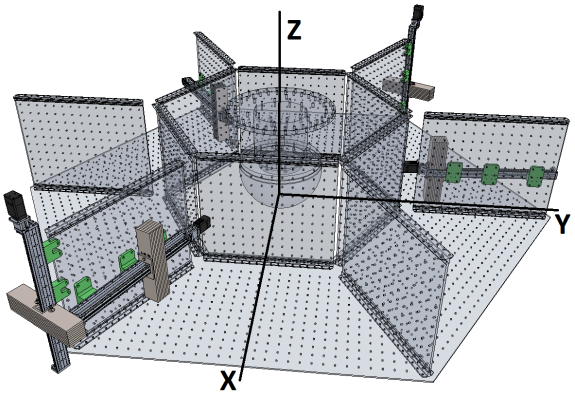

Figure 1. Computer illustration of the actuator locations and coordinate system

1.6 Research Objectives and Methodology

The need exists to design a system, upon a coarse manual balancing effort, that will balance the platform with actuated masses. This research looks at ways of implementing a dynamic system to balance the ACSPG. A dynamic system will improve the initial manual balancing process, which occurs frequently as the ACSPG is reconfigured. Improving the balancing process allows for better utilization of resources.

It is assumed gravity is the primary cause of undesirable torques, and is the focus of the control system which drives the DMBS. Following work applied to other simulators, there are two proposed courses of action. The first is to solve for the required control torque on the system due to the offset of the COM relative to the COR. The second is to determine the offset of the centroid with a least squares estimation approach and map this offset to the sliding masses.

The collected data is assumed as accurate enough to allow for the software to precisely measure accelerations to determine the distance between the COM and COR and torques created. This is determined in Matrix Laboratory (MATLAB) using the ordinary differential equation (ODE) solver ode45 and the dynamic equations presented later in this paper. Several simulation iterations evaluate the effectiveness of the algorithms. The scope of this paper is limited to simulations of the movement of the sliders. Future work is required to develop an internal control to move the sliding masses.

1.7 Thesis Overview

In the following chapters, this thesis thoroughly investigates the objective of balancing the platform through model development, simulation, and analysis. Chapter II details literature regarding attitude control and mass balancing systems

and the application of this previous research to solve the stated objectives. Chapter III discusses the ACSPG's configuration, how the mass balancing system was designed, and explores the dynamics required to determine the position of the COM relative to the COR. Chapter IV presents the algorithms implemented and reviews the data acquired during simulations. Chapter V summarizes the findings and presents future research paths.

II. Background

2.1 ACSPG Overview

Improving the balancing process of the ACSPG allows for longer simulation times, improving data collection. This is important because the results of these tests are applied to the design of attitude control systems for use in space. Utilizing data from on-board inertial measurement units (IMUs), angular accelerations and velocities are captured and processed by the flight computer. Currently this data is used in conjunction with a motion capture system in determining the ACSPG's orientation as explained by Penn and Reifler [8]. A MATLAB model of the ACSPG's control system is used to model and simulate its attitude. A computer-generated model of the ACSPG is presented in Figure 2.

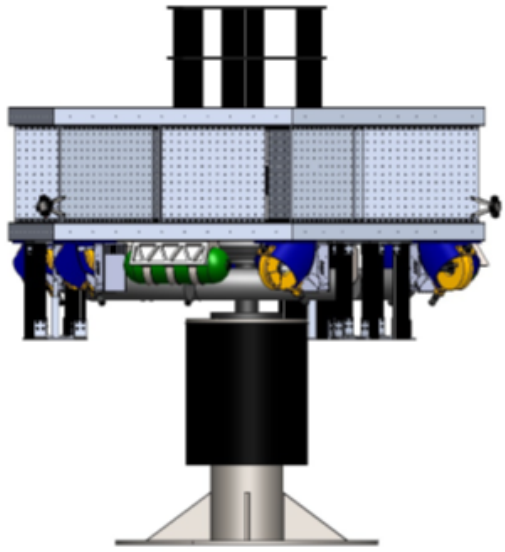

Figure 2. Computer rendering of the ACSPG

2.2 Use of Satellite Simulators

Controlling the attitude of spacecraft was a concern nearly as long as spacecraft have existed. Testing is conducted in order to verify the performance of the attitude control systems. This is done on test beds, on either planar tables for evaluating mating and docking maneuvers, or rotational air bearings for attitude and control tests. Planar tables allow for three translational degrees of freedom (DOF) along the x, y, and z-axes. Air bearings allow for three rotational DOF, roll, pitch, and yaw, as detailed by Kim and Agrawal [6]. In certain cases, they are combined to provide six DOF [4]. By utilizing air bearings, laboratories are able to create a nearly torque-free environment. While their performance is not perfect, the experiments they allow for are conducted in as close to a microgravity environment as possible [9].

Stanford University, by modifying a planar system, was the first academic facility to develop an air bearing platform. Stanford used their air bearing platform for identifying the center of masses of objects in 1975 [4]. There is a high likelihood of earlier usage in the government and private sector. However, there is limited documentation available for early air bearings due to the secretive, classified, and proprietary nature of the equipment at these facilities [4].

These institutions primarily utilize air bearings to reduce the effects of friction during attitude control experimentation. Friction is a resistive force, preventing translation or rotation between two surfaces [10]. The sheet of air forced between the two surfaces substantially reduces the frictional force normally making control of the simulator more difficult. The typical setup of an air bearing test platform consists of two spherical or hemispherical surfaces creating a ball and socket type of joint. They are separated by highly pressurized air flowing up through and out of one sphere, creating a thin region of air between them as indicated by the hatching

in Figure 3. While some systems utilize a magnetic suspension system, their limited range of motion relative to air bearings reduces the usefulness of magnetic suspension in many applications. One requirement of platforms is minimizing any deviations of distance between the center of the air bearing and COM, while maintaining a maximum level of range of motion in each axis [4].

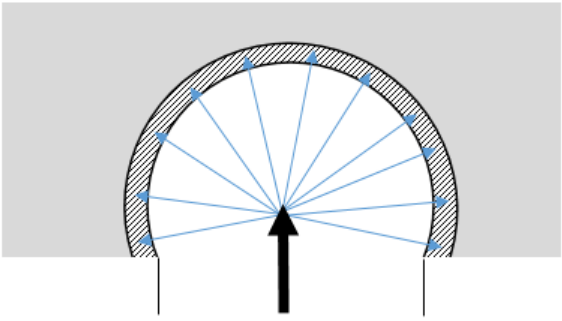

Figure 3. Air flow through bearing, where the hatched area represents a thin sheet of air separating the two bodies

Early air bearing platforms were the size of tables holding similarly small payloads. In the 1990s, AFRL, then the Astronautics Laboratory under Air Force Systems Command, developed the Advanced Space Structure Technology Research Experiments (ASTREX) facility with an 18 inch diameter air bearing, capable of supporting payloads over 14,500 pounds [11]. AFIT's SIMSAT, and other similarly used platforms are much smaller. These platforms support much smaller payloads, typically hundreds of pounds [12]. The ACSPG is much larger than the typical air bearing setup, though not quite as large as the ASTREX. These smaller platforms have undergone work to create balancing systems for their usage. The ACSPG is one of the largest test platforms of its kind in the world. Its size dictates a mass balancing system capable of responding to its substantial inertia.

Housing air bearing platforms in proper facilities is important. It is necessary to control and mitigate other environmental torques. G. Allen Smith identified several

additional factors not normally considered in the analysis of platform dynamics. Those factors include the changing MOI from the elasticity of the platform as it flexes under gravity, air currents in the laboratory, and magnetic fields generating electromagnetic torques, as well as imbalances caused by wiring and battery discharges [13]. He also discussed the importance of developing an automatic balancing system stating three weights on orthogonal axes, driven by linear actuators can accomplish this.

2.3 Fundamentals of Attitude Control

Any discussion of motion and inertia traces its history back to Issac Newton. The physical laws governing the motion of the ACSPG are founded in his works. His third law of motion is simplified as, "every action results in an equal and opposite reaction." Momentum exchange devices, such as CMGs, rely and this principal in controlling spacecraft and see use on the ACSPG [14].

A CMG consists of a spinning flywheel rotating on a gimbaled axis. As the wheel is tilted, angular momentum is transferred into the platform. Where the angular momentum of a system $\vec{H}$ is defined by

$$\vec{H} = \bar{J}\vec{\omega} \tag{2.1}$$

Where $\bar{J}$ is the MOI tensor and $\vec{\omega}$ is the angular velocity of the rotating body. When implemented in the design of spacecraft, CMGs are used to either generate rotation for a slewing maneuver or to change the attitude of the spacecraft [2]. This allows for operational maneuvers such as aiming cameras at stars, pointing radios at ground stations, or exposing solar panels to the sun. Similarly, if an unwanted external torque is present, the CMGs are used to counteract this torque.

The ACSPG has CMGs for minor attitude stabilization. A concern with CMGs is they can only rotate up to 180 degrees before they encounter a singularity and are no longer able to provide the necessary torque [15]. This limitation is not found in reaction wheels (RWs), which are another mean of attitude control. Varying the speed of the wheel varies the torque it generates. As the RWs spin faster, they generate greater torques, but the speed of the wheels are mechanically limited and they can become saturated. The saturation of a RW refers to it reaching the maximum rotational velocity of the motor and its limit for storing momentum. Variable speed CMGs (VSCMGs) combine the capabilities of CMGs and RWs by allowing for adjusting the speed of the wheel and adjusting the orientation of the gimbal. To eliminate the limitations of CMGs and RWs, studies have focused on the number and arrangement of CMGs [5].

2.3.1 Application of MOI Calculations to the ACSPG

The ACSPG rotates on a large hemispherical air bearing. Various computers and sensors are used for gathering experimental data and controlling the motion of the ACSPG. The automated balancing system will comprise of actuators and sliding masses in the vertical and horizontal directions. For mathematical purposes, the center of the air bearing is used as the COR and the origin for the body and inertial frame coordinate systems. The COM, also known as the centroid, is the point about which the system balances. It is the average position of all the mass in an object, calculated with Equation 2.2

$$\frac{\sum m_i \vec{r}_i}{\sum m_i} = \frac{m_1\vec{r}_1 + m_2\vec{r}_2 + m_3\vec{r}_3 + m_4\vec{r}_4 + m_5\vec{r}_5 + M_{ACSPG}\vec{r}_{ACSPG}}{m_1 + m_2 + m_3 + m_4 + m_5 + M_{ACSPG}} \tag{2.2}$$

where m_i represents each sliding mass and $\vec{r}_i$ is the position of the mass relative to the origin. The total mass of the ACSPG, not including the sliding masses, is

represented by M_{str}. The location of the COM of the ACSPG, not including the sliding masses, is represented below by $\vec{r}_{str}$.

Before experimentation begins, operators attempt to balance the static system by adding incremented masses as accurately as possible. After experimentation on the ACSPG begins, any slight deviations between the COR and COM are instantly realized, and the platform tilts. The CMGs are used to counter the gravitational torques and keep the platform balanced. Unfortunately the CMGs quickly reach saturation, resulting in shortened experiments. Not only will the mass balance system provide a more accurate initial starting point, as it evolves into a dynamic system, it will maintain the COM and COR alignment,enabling longer experimental run times.

2.4 Mass Balance Systems in Use

Two overarching designs exist for configuring mass balance systems. The primary layout involves aligning masses orthogonally along the Cartesian coordinate axes, as seen in Figure 4. This allows for direct mapping of deviations between the COM and COR and the location of the masses. To a lesser extent, non-orthogonal configurations, like the ACSPG and one at Harbin Institute of Technology (HIT), are used as an alternative to the widely used orthogonal configuration [1].

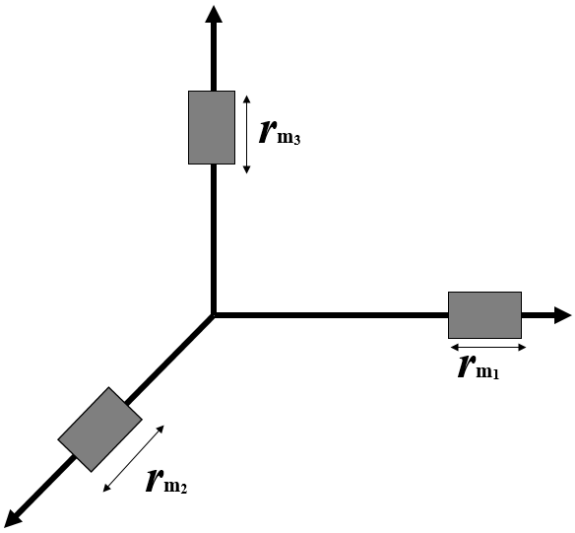

Figure 4. Mass balancing system with Cartesian coordinates [1]

Sliding masses as a means of stabilization is not just limited to ground based simulators. Moving masses to adjust the center of mass is a topic also seeing application for spacecrafts in orbit. Shifting weights in a linear fashion directly affects the MOI, when used in conjunction with reaction wheels and magnetorquers allows for attitude control of the spacecraft. The torques encountered in the space environment are different than those on earth, however system stabilization is important in both situations [16].

2.5 Orthogonal Configurations

Utilizing an orthogonal configuration, NPS has performed substantial analysis on balancing spacecraft simulators [7]. With their orthogonal configuration, masses move either parallel or perpendicular to the gravitational field. One challenge encountered was simultaneously estimating torques parallel and perpendicular to the gravitational field. If a mass is moved perpendicular to the gravitational field, and the estimator is relying upon the ability to calculate torques parallel with the

gravitational field, the feedback provided to the system is not very beneficial. NPS determined this is overcome by implementing a two step procedure.

To determine the positioning of the sliding masses, NPS developed a nonlinear adaptive control. The control initially accounts for offsets in the horizontal plane. As the nonlinear adaptive control estimates the offsets perpendicular to the gravitational field, sliding masses compensate for the estimated offset creating a control torque. The control torque alters the angular velocity of the platform, which is then used to continually update the offset estimation. As the error of the offset estimation converges to zero, the angular velocities about the two horizontal axes converge to zero, indicating the control has compensated for the offset perpendicular to the gravitational field.

Upon determining the offset in the transversal direction, a Kalman filter is employed to estimate the offset in the direction parallel to the gravitational field. When evaluating both UKF and extended Kalman filter (EKF) performance, NPS determined the performance of both filtering methods was similar. Applying an UKF the vertical offset is estimated, which is compensated for by adjusting the vertical sliding mass.

By aligning the balancing actuators with the principal axes of rotation, the researchers at NPS are able to simplify their calculations. This assumption ensures the MOI matrix remains diagonal. Furthermore, the assumption is made that changes to the MOI are negligible due to the small size of the sliding masses relative to the system, $\dot{\bar{J}} = 0$ [7].

At the HIT, a six degree of freedom simulator was designed to account for both planar and rotational motion. Yan, *et al.*, explore various mass balancing system configurations. They originally looked at an orthogonal configuration, having masses arranged similar to three dimensional Cartesian coordinates, aligning one

mass vertically and two aligned along the two perpendicular axes which create a horizontal plane. When testing filtering methods, HIT favored an UKF. Similar to NPS, the adaptive control system at HIT compensates for offsets perpendicular to the gravitational field and then accounts for vertical offsets. Using proper Lyapunov function, the closed loop control system is verified as stable, allowing for the balancing of the system [17].

2.6 Non-orthogonal Layouts

In addition to the above mentioned orthogonal configuration, other researchers at HIT tested a non-orthogonal mass balancing configuration. Arranging their masses symmetrically around the center, when viewed from above, the three translational axes of the masses create an appearance shown in Figure 5. To account for vertical imbalance, the masses are inclined at 30 degrees.

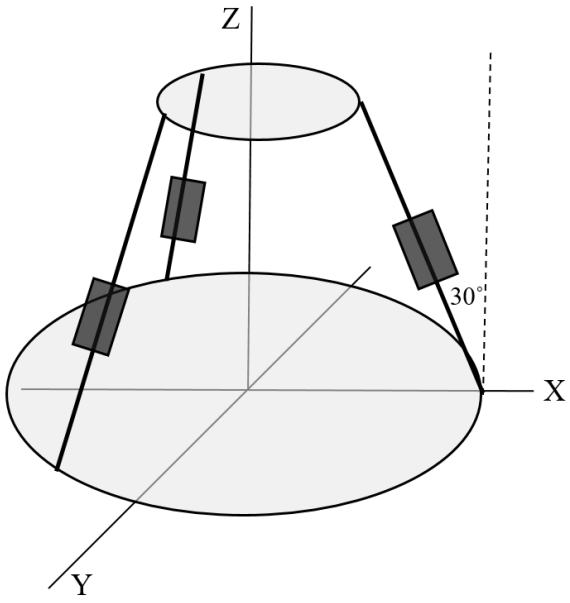

Figure 5. Harbin Institute of Technology mass configuration [1]

HIT researchers determined the symmetrical arrangement, as well as aligning the translational axes with the COR, simplifies the geometry of the system and the needed calculations. When modeling and calculating the mass locations, HIT assumes the masses are ideal point masses, an assumption also used in this study [17]. When automatically balancing the test bed via a non-orthogonal configuration a recursive least squares approximation is utilized [1].

The least-squares method is employed by integrating the output angular accelerations to determine the centroid. By performing experiments HIT evaluates this methodologies effectiveness in estimating the COM offset. The masses are adjusted ensuring coincidence between the COM and the COR. They include the Coriolis effects to ensure all possible sources of rotation are accounted for [17, 1]. While this research does not consider the Coriolis effect, including it will improve the accuracy of future designs.

Utilizing Euler angles, HIT defines two coordinate systems, an inertial coordinate system and a body fixed coordinate system, which rotates with the platform. With the defined kinematics of the system, there exists a singularity when the roll or pitch angle exceeds 90 degrees. Fortunately, the dynamics of the system prevent it from rotating beyond 30 degrees in either direction. Applying Euler angles, this also requires consideration. The ACSPG similarly benefits with its similar rotational limits.

2.7 Mass Balancing at AFRL

Through simulations conducted by AFRL, several configurations for the mass balance system (MBS) were evaluated. Different layouts were simulated on their ability to account for deviations of the COM relative to the COR. The chosen configuration allows for the largest region of coverage of movement of the COM.

AFRL's design features three linear actuators in the horizontal x-y plane, separated by 120 degrees, and two linear actuators positioned vertically. Wang, *et al.* employee a nonlinear control method similar to the one introduced by Chesi and presented in this thesis for application to the ACSPG [17].

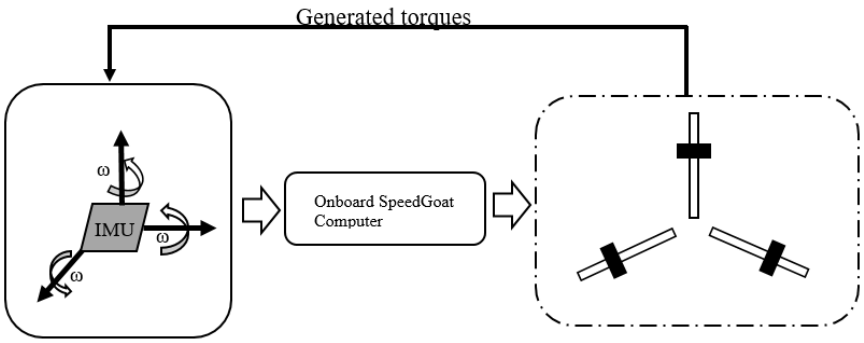

Figure 6. ACSPG feedback control loop

Upon calculating the centroid deviation, the required displacement of each slider requires calculation. Upon moving the sliding masses, the centroid changes. The system can iterate the process to determine additional changes required to properly align the centroid with the COR [1]. The feedback loop is represented in Figure 6 demonstrating as the masses move, torques on the system change, resulting in changes in the angular velocities accelerations. The IMU detects the changes, which are fed into the onboard computer directing new positions for the masses.

2.8 Dynamics Overview

The fundamental problem of balancing the platform, is in its simplest form, similar to balancing a seesaw. When the centroid and COR are co-located the system is balanced. When the COM does not align with the COR, an gravitational torque exists. Adjusting the position of sliding masses allows for creating a control torque to counteract the torque from the offset between the COM and the COR. As

the position of the sliding mass changes, so too does the location of the COM. As the angular rates are measured in the body frame, it is necessary to convert between the inertial frame and the body frame.

The moment of inertia of a system and its first derivative are calculated by Equation (2.3a) and Equation (2.3b),

$$\bar{J} = \sum_{i=1}^{n} m_i \vec{r}_i{}^2 \tag{2.3a}$$

$$\dot{\bar{J}} = \sum_{i=1}^{n} 2 m_i \vec{r}_i \frac{d\vec{r}_i}{dt} \tag{2.3b}$$

where m_i represents the i^{th} point mass in the body and $\vec{r}$ is the position vector of the mass relative to the center of the body. For a rigid body in the inertial frame angular momentum is represented as

$$\vec{H}_I^c = \bar{J}_I^C \vec{\omega}_I^{BI} \tag{2.4}$$

where the angular velocities ω and accelerations $\dot{\omega}$ are extracted from the IMUs and allow for conversion from between the body frame and the inertial frame. Knowing the moment or torque of a system is the first time derivative of the angular momentum yields [18]

$$\vec{L} = \sum_{i=1}^{n} \vec{F}_i \vec{r}_i = \bar{J}\dot{\vec{\omega}} + \dot{\bar{J}}\vec{\omega} \tag{2.5}$$

As long as changes to the mass positions remain small, $\dot{\bar{J}}$ is assumed as zero. When the system is balanced, angular accelerations no longer exist, and all torques on the system offset each other.

2.9 Lyapunov's Direct Method

Due to a readily available candidate Lyapunov function, Lyapunov's direct method is used to demonstrate convergence of a nonlinear system upon an equilibrium point [18]. For an autonomous nonlinear system $f(x) = \dot{\bar{x}}$ Lyapunov's method requires satisfying three conditions to prove the candidate function is a positive definite scalar function. First, there must exist an equilibrium value (often denoted as $\bar{x}^*$ or $\bar{x}_e$) where the function equals zero. Second, the function requires a value greater than zero for all other conditions. Third, for all values other than the the equilibrium value, the first derivative of the function must equal or less than zero [19]. These conditions are summarized as:

1) $V(\bar{x}^*) = 0$

2) $V(\bar{x}) > 0$ for all $\bar{x} \neq \bar{x}^*$

3) $\dot{V}(\bar{x}) \leq 0$ for all $\bar{x} \neq \bar{x}^*$ and all future time

Satisfying all three conditions is necessary properly determine the stability of a system using Lyapunov's direct method.

2.10 Unscented Kalman Filters

When the states of a system are not measurable, the states require estimating. Due to its ease of use the Kalman filter (KF) is widely used for linear models. The EKF was introduced to linearize nonlinear models. Difficulty arises in the EKF's implementation as deriving the required Jacobian matrix or tuning it present challenges. The UKF was introduced by Julier and Uhlman to provide an elegant method for estimating nonlinear systems. Using noisy data, taking estimations from multiple sensors allows for estimating the true state [20].

The UKF uses an unscented transform within a Kalman Filter to transform states from one coordinate system to another. Using prior states, a model is

implemented to predict the next state. That state is measured and compared against the original estimation to update the initial estimation method. Using the new state, the next state is estimated utilizing the refined predictive model and the process is repeated. Covariance between sampled points is propagated through the model as deterministic sampling is used to pick sigma, or weighted, points through the nonlinear transformations. As each state updates, the generated data is used to constantly update the predictions [21].

2.11 Implementation Challenges

The determined COM is based upon calculations and estimations, all containing error levels. Properly determining the offset requires minimizing this error through accurate gathering of information. Error can exist in inaccurate mass and MOI values, actuator calibration, and external disturbances [6]. Perfection is not required as long as the gravitational torques are reduced to within the limits of other attitude control systems in place.

Recursive estimation methods can provide good initial calculations. Upon the repositioning of the masses, the control loop is continuously rerun, working to ensure proper convergence. In other words, a prediction is made for the final position. However, until the masses are moved, the system might not have properly predicted the final location. This results in continual calculations to ensure stability. Initial calculations are also made based on fixed locations of the items on the simulator. As cables shift, structures flex, and components vibrate, additional disturbances to the system develop. This creates a problem in verifying the accuracy of the mass balancing system's results [6].

2.12 Summary

This chapter first reviewed previous work performed with satellite simulators. It then discussed the fundamentals behind attitude control and mass balancing systems. It reviewed applications of orthogonal and non-orthogonal mass balancing layouts. Finally, it identified challenges for consideration when implementing a mass balancing system. Chapter III will discuss the process and procedures used in the design and implementation of a mass balancing system model.

III. Methodology

This chapter begins by describing the equipment used in the mass balancing system. Next, two techniques for balancing the system are presented. Following those is a method for applying the controls to the non-orthogonal configuration. Finally, this chapter discusses how the presented methods are evaluated for application on the ACSPG. A comparison of the two methods is performed, first evaluating a nonlinear control as applied to a simulator at NPS and a recursive least squares approach as utilized in other locations.

3.1 Overview

The focus of this research is developing a control algorithm for the ACSPG for the implementation of an automated balancing system. The development of the mass balancing system consists of three fundamental steps. The first is developing the control algorithm to efficiently reposition the masses. The second is applying this control to the non-orthogonal configuration of the sliding masses. The final step is characterizing the linear actuators responsible for adjusting the masses, meaning their physical capabilities and performance need determining, however, due to time limitations, characterizing the motion is not the focus of this research.

3.2 ACSPG Equipment

The motion of the ACSPG is controlled by a Speedgoat computer optimized for operating the code AFRL developed in Simulink^{TM}. Several pairs of air nozzles simulate on-orbit thrusters capable of rotating the platform. CMGs surround the system to mitigate unwanted torques as they develop during experimentation. The entire system is self-contained and powered by batteries to avoid wires extending to

external systems, potentially restricting motion and impeding performance. All necessary communication between external and on board systems is performed via radio frequency communication. IMUs are used in determining the attitude of the system. The mass balancing system comprises of five masses, each sliding along a linear actuator, three horizontally and two vertically.

3.2.1 IMUs

The IMUs detect angular velocities with internal accelerometers and gyroscopes and allow for determining angular accelerations. This information is captured in the body frame as changes in angles Φ, Θ, and Ψ, which are the angles rotated about the x, y, and z- axes respectively. Each measurement from the IMU has a small amount of error, which has the potential to compound over time. However, the angular velocities and accelerations are filtered by the on board computer to provide more accurate measurements without the compounded error.

3.2.2 Linear Actuators

The linear actuators are responsible for moving the masses in a prescribed manner. Each linear actuator consists of a high torque Moog Animatics SmartMotor^{TM} capable of driving a 3/8 inch threaded shaft 600 mm in length, as pictured in Figure 7. Actuators slide the 20 kg masses to their desired locations. Each mass is comprised of eight steel plates.

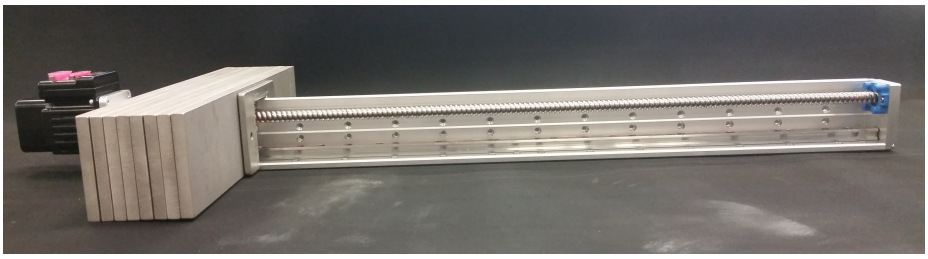

Figure 7. Profile view of actuator assembly

During the initial development of the control system, the acceleration of the actuators is assumed as instantaneous. In reality, the motion is more accurately profiled as a ramp function, where the mass accelerates to the desired speed. AFRL is characterizing the performance of the actuators and determining the profile of the motion to determine the response of the actuators to inputs. The movement of each mass is also limited by the length of the actuator. Limits, such as actuator length, are incorporated into the control system, without which, the model could easily exceed the physical capabilities of the design.

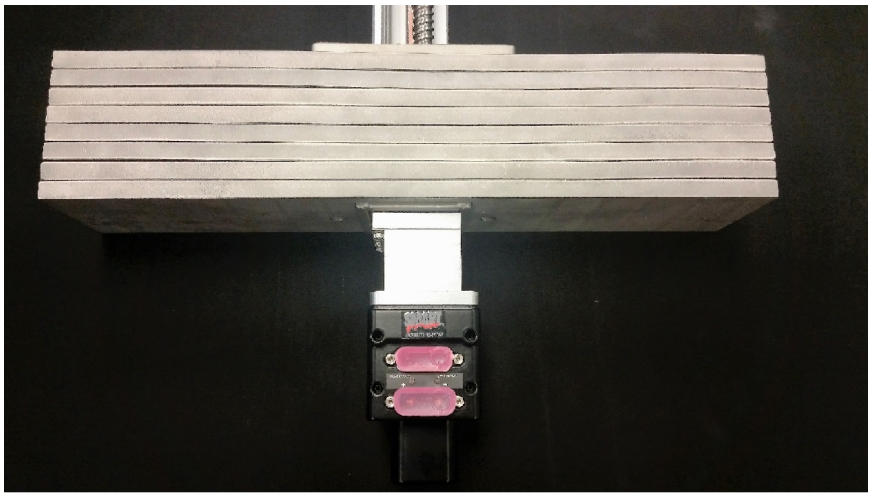

Figure 8. The motor and the mass assembly

3.3 Nonlinear Control Law Utilizing an UKF

This section describes the method for implementing a non-linear control law. The control law is determined with a two-step process. First, the control law compensates for the torques caused by offsets in the horizontal plane and perpendicular to the gravity field. Second, the vertical offsets parallel to the gravitational field are compensated for. The offset between the COM and COR is represented by the position vector $\vec{r}_{\text{off}} = [r_{\text{off},x}\ r_{\text{off},y}\ r_{\text{off},z}]^T$. Before any balancing efforts, any non-zero value of r_{off} causes a torque to exist. For the purposes of this research, r_{off} is simulated, the controller then estimates the offset as $\hat{r}_{\text{off}}$, and the estimate is verified as accurate when the error of the estimate, $\tilde{r}_{\text{off}}$ equals zero.

3.3.1 Horizontal Balancing

To develop the control law in the horizontal plane, this research follows the procedure outlined by Chesi, *et al.* [7]. The angular momentum of the ACSPG is represented by

$$\vec{H} = \bar{J}\vec{\omega} \tag{3.1}$$

and the first derivative is

$$\dot{\vec{H}} = \dot{\bar{J}}\vec{\omega} + \bar{J}\dot{\vec{\omega}} \tag{3.2}$$

where $\bar{J}$ is the inertia tensor of ACSPG and ω is the angular velocity, and this is the torque on a body. The motion of the sliders is assumed small and does not contribute to changes in the MOI, $\dot{\bar{J}} = 0$. The assumption of a constant MOI requires further consideration with a simulator with the mass properties of the ACSPG. As long as the masses remain fixed, the dynamics of the simulator follow Euler's equation of motion for a rotating body [7]

$$\dot{\vec{H}} + \vec{\omega} \times \bar{J}\vec{\omega} = \vec{r}_{off} \times m_{str}\vec{g}^{\,b} \tag{3.3}$$

where m_{str} is the mass of the simulator structure, and $\vec{g}^{\,b}$ is the gravity vector in the body frame. To compensate for imbalances, the system requires the introduction of a control torque, $\bar{\tau}_r$. Adjusting the position of the masses provides the needed control to obtain a balanced system. As such, Equation (3.3) is rewritten to include the torque as

$$\dot{\vec{H}} + \vec{\omega} \times \bar{J}\vec{\omega} = \vec{r}_{off} \times m_{str}\vec{g}^{\,b} + \vec{\tau}_r \tag{3.4}$$

Let the control torque be [7]

$$\vec{\tau}_r = m_{str}[\vec{g}^{\,b}\times]\hat{\vec{r}}_{off} - k_p\vec{w}_p \tag{3.5}$$

where $[\vec{g}^{\,b}\times]$ is the skew-symmetric matrix used to represent a cross product for matrix multiplication defined as

$$[\vec{g}^{\,b}\times] = \begin{bmatrix} 0 & -g_z{}^b & g_y{}^b \\ g_z{}^b & 0 & -g_x{}^b \\ -g_y{}^b & g_x{}^b & 0 \end{bmatrix} \tag{3.6}$$

and the estimated position vector of the COM is represented as $\hat{\vec{r}}_{off}$ and k_p is a tunable gain. Let $\kappa = -m_{str}[\vec{g}^{\,b}\times]$.

Substituting κ into Equation (3.3)

$$\bar{J}\dot{\vec{\omega}} + \vec{\omega} \times \vec{J}\vec{\omega} = -\kappa\vec{r}_{off} + \vec{\tau}_r \tag{3.7}$$

and then including Equation (3.5) and rewriting produces

$$\bar{J}\dot{\vec{\omega}} + \vec{\omega} \times \bar{J}\vec{\omega} = -\kappa\vec{r}_{off} + \kappa\hat{\vec{r}}_{off} - k_p\vec{w}_p \tag{3.8}$$

which is simplified as

$$\bar{J}\dot{\vec{\omega}} + \vec{\omega} \times \bar{J}\vec{\omega} = -\kappa(\vec{r}_{off} - \hat{\vec{r}}_{off}) - k_p\vec{w}_p \tag{3.9}$$

The estimated error of the position vector between the COM and COR is the true value of the position vector minus the estimated value of the position vector, defined by

$$\tilde{\vec{r}}_{off} = \vec{r}_{off} - \hat{\vec{r}}_{off} \tag{3.10}$$

Equation (3.9) is rewritten as

$$\bar{J}\dot{\vec{\omega}} + \vec{\omega} \times \bar{J}\vec{\omega} = \kappa(\tilde{\vec{r}}_{off}) - k_p\vec{w}_p \tag{3.11}$$

Rearranging this to solve for $\dot{\vec{\omega}}$ produces the closed loop equation

$$\dot{\vec{\omega}} = \bar{J}^{-1}[-\vec{\omega} \times \bar{J}\vec{\omega} + \kappa(\tilde{\vec{r}}_{off}) - k_p\vec{w}_p] \tag{3.12}$$

To appropriately rotate gravity from the inertial frame to the body frame, the following is used

$$\vec{g}^{\,b} = R_i^b \times \vec{g}^{\,i} \tag{3.13}$$

where gravity in the inertial frame is defined as $\vec{g}^{\,i} = \begin{bmatrix} 0 & 0 & -9.81 \end{bmatrix}^T m/s^2$, and R_i^b is the rotation matrix defined as

$$R_i^b = \begin{bmatrix} 1-2(q_2^2+q_3^2) & 2(q_1q_2-q_4q_3) & 2(q_1q_3+q_4q_2) \\ 2(q_1q_2+q_4q_3) & 1-2(q_1^2+q_3^2) & 2(q_2q_3-q_4q_1) \\ 2(q_1q_3-q_4q_2) & 2(q_1q_3+q_4q_1) & 1-2(q_1^2+q_2^2) \end{bmatrix} \tag{3.14}$$

where $q_{1:4}$ represents each term from the attitude quaternion. The current research assumes that the quaternion attitude information is properly filtered and with minimal error.

3.3.2 Stability Verification Using Lyapunov's Direct Method

Upon determining the control law for the system, the need exists to prove the control law guarantees stability. Stability is demonstrated using Lyapunov's direct method [18]. Restating the three required conditions from Section 2.9 where V is a scalar:

1) $V(\bar{x}^*) = 0$

2) $V(\bar{x}) > 0$ for all $\bar{x} \neq \bar{x}^*$

3) $\dot{V}(\bar{x}) \leq 0$ for all $\bar{x} \neq \bar{x}^*$ and all future time.

Assuming the candidate Lyapunov function of the form [7]:

$$V(\bar{x}) = \frac{1}{2}\omega^T \bar{J}\omega + \frac{1}{2}\tilde{r}_{off}^T r_{off} + \frac{1}{2}q^T q \tag{3.15}$$

where $\bar{x} = [q, \omega, \tilde{r}_{off}]^T$. When $\bar{x} = 0$, $V(\bar{x}) = 0$, which satisfies the first condition. For positive values of $\bar{x}$, $V(\bar{x}) > 0$, satisfying the second condition. To prove the third condition, the time derivative of the original function is taken as

$$\dot{V}(\bar{x}) = \vec{\omega}^T \bar{J}\dot{\vec{\omega}} + \tilde{r}_{off}^T \dot{\tilde{r}}_{off} + q^T \dot{q} \tag{3.16}$$

With $q^T\dot{q} = 0$ this combines with Equation (3.11) to allow for rewriting the above as

$$\dot{V}(x) = \vec{\omega}^T(-\vec{\omega} \times \bar{J}\vec{\omega} + \kappa\vec{r}_{off} + \vec{\tau}_r) + \tilde{r}_{off}^T\dot{\tilde{r}}_{off} \tag{3.17}$$

where $\dot{\tilde{r}}_{off} = -\kappa^T\vec{\omega}_g$. Let $\vec{\omega} = \vec{\omega}_g + \vec{\omega}_p$ where ω_p are the two angular velocity components perpendicular to $\vec{g}^{\,b}$ and $\vec{\omega}_g$ is the angular velocity component parallel to $\vec{g}^{\,b}$ [16]. Substituting and rearranging, this is rewritten as

$$\dot{V} = -k_p(\vec{\omega}_g + \vec{\omega}_p)^T\vec{\omega}_p \tag{3.18}$$

where $\vec{\omega}_g^T\vec{\omega}_p = 0$ due to their perpendicular nature, so,

$$\dot{V} = -k_p||\vec{\omega}_p||^2 \leq 0 \tag{3.19}$$

satisfying the third condition, indicating closed loop stability.

Using LaSalle's invariance principle to determine the largest invariant set [7]

$$\{\dot{V}(t) \equiv 0\} = \{\bar{X} : \dot{V}(\bar{q}, \vec{\omega}, \tilde{r}_{off}) \equiv 0\} = \{\bar{\omega}_p(t) = 0\} \tag{3.20}$$

To determine if the estimator converges:

$$\dot{\hat{r}}_{off} = \kappa^T\vec{\omega} = \kappa^T(\vec{\omega}_p + \vec{\omega}_g) = \kappa^T\vec{\omega}_p + \kappa^T\vec{\omega}_g \tag{3.21}$$

By LaSalle, the system will converge on the largest invariant set in $\{\bar{\omega}_p = 0\}$ where $\dot{\hat{r}}_{off} = \kappa^T\bar{\omega}_g$. Because $\vec{\omega}_g$ is perpendicular to κ^T, $\dot{\hat{r}}_{off} = 0$.
Knowing

$$\vec{\omega}_p = P_p(q)\vec{\omega} = \left[\mathbb{I} - \frac{\vec{g}^{\,b}(\vec{g}^{\,b})^T}{||\vec{g}^{\,b}||^2}\right]\vec{\omega} \tag{3.22}$$

where $\mathbb{I}$ is the identity matrix and P_p is a projection matrix. If $\vec{\omega}_p = \begin{bmatrix} 0 \\ 0 \\ 0 \end{bmatrix}$ then

$$P_p = \begin{bmatrix} 1 & 0 & 0 \\ 0 & 1 & 0 \\ 0 & 0 & 1 \end{bmatrix} - \begin{bmatrix} g_x^2 & 0 & 0 \\ 0 & g_y^2 & 0 \\ 0 & 0 & g_z^2 \end{bmatrix} \begin{bmatrix} \omega_1 \\ \omega_2 \\ \omega_3 \end{bmatrix} \frac{1}{||g_b||^2} = \begin{bmatrix} 1 & 0 & 0 \\ 0 & 1 & 0 \\ 0 & 0 & 0 \end{bmatrix} \tag{3.23}$$

As this is a rotation about z^b, g_x^b and g_y^b converge to 0. Then

$$P_p\dot{\vec{\omega}} = \frac{d}{dt}(P_p\vec{\omega}) = \dot{\vec{\omega}}_p = P_pJ^{-1}(\vec{\omega} \times J\vec{\omega} + \kappa\tilde{r}_{off} - k_p\vec{\omega}_p) \tag{3.24}$$

which is simplified as

$$0 = P_pJ^{-1}(-\vec{\omega}_g \times J\vec{\omega}_g + \kappa\tilde{r}_{off}) \tag{3.25}$$

Assuming $\bar{J}$ is diagonal and movement of the sliding masses will not alter the principal axes so $\vec{\omega}_g \times \bar{J}\vec{\omega}_g = 0$. This allows for rewriting Equation (3.25) as

$$0 = P_pJ^{-1}(\kappa\tilde{r}_{off}) \tag{3.26}$$

κ is given as $\kappa = -m_{str}\begin{bmatrix} 0 & -g_z^b & g_y^b \\ g_z^b & 0 & -g_x^b \\ -g_y^b & g_x^b & 0 \end{bmatrix}$, but for $\omega_p = 0$, it must also be true that $g_x^b = g_y^b = 0$.

Rearranging,

$$\begin{bmatrix} 0 \\ 0 \\ 0 \end{bmatrix} = -m_{str}\begin{bmatrix} 1 & 0 & 0 \\ 0 & 1 & 0 \\ 0 & 0 & 0 \end{bmatrix}\begin{bmatrix} J_{xx}^{-1} & 0 & 0 \\ 0 & J_{yy}^{-1} & 0 \\ 0 & 0 & J_{zz}^{-1} \end{bmatrix}\begin{bmatrix} 0 & g_z^b & 0 \\ -g_z^b & 0 & 0 \\ 0 & 0 & 0 \end{bmatrix}\begin{bmatrix} \tilde{r}_{off,x} \\ \tilde{r}_{off,y} \\ \tilde{r}_{off,z} \end{bmatrix} \tag{3.27}$$

This is rewritten as

$$0 = J_{xx}^{-1} g_z^b \tilde{r}_{off,y} \tag{3.28a}$$

$$0 = -J_{yy}^{-1} g_z^b \tilde{r}_{off,x} \tag{3.28b}$$

$$0 = 0 \times \tilde{r}_{off,z} \tag{3.28c}$$

Knowing $J_{xx} \neq 0$, $J_{yy} \neq 0$, and $g_z^b \neq 0$ it follows for these equations to be true, $\tilde{r}_{off,y} = \tilde{r}_{off,x} = 0$. Equation (3.28c) is an identity and does not provide any information regarding $r_{off,z}$. Because of this, $r_{off,z}$ requires determination by other means. The nonlinear adaptive control law is Lyapunov stable in the horizontal plane and estimates the horizontal components of r_{off} once on the invariant set, but is unable to estimate the vertical component of r_{off}.

3.3.3 Vertical Balancing

As explained in subsection 3.3.2, the offsets in the vertical direction were indeterminable. To estimate offsets in the vertical direction, an UKF is used. Filtering allows for attitude determination by taking measurements containing error and noise, assuming a probability distribution, and estimating biases to remove those biases from the state estimates [18].

The state space equations are

$$\dot{\vec{\omega}} = \bar{J}^{-1}(-\vec{\omega} \times \bar{J}\vec{\omega} + \vec{d}) \tag{3.29}$$

where $\vec{d}$ is a disturbance torque

$$\vec{d} = \begin{bmatrix} -m_{str} \cdot g_y^b \cdot r_z \\ m_{str} \cdot g_x^b \cdot r_z \\ 0 \end{bmatrix} \tag{3.30}$$

The state space equations are implemented in MATLAB with an UKF and evaluated at varying time step sizes to determine its ability to quickly estimate the offset in the vertical direction. Any vertical offset is directly mapped to a precise displacement needed by the two coupled vertical balancing masses.

3.4 Recursive Least Squares

Another method implemented in mass balancing systems involves a recursive least squares approach. By weighting measured values, a deterministic approach is utilized for calculating the offset between the COM and COR. Where the previous method employed use of quaternions in determining the attitude this method is solved using the Euler angles. The presented method follows that as detailed by HIT [1]. A true comparison of the balancing methods requires utilizing quaternions

3.4.1 Least Squares Equation Transformation

The inertial frame is located at the center of the simulator and at the beginning of the simulation (at $t_0 = 0$) the body frame is co-located to align with the inertial frame of the simulator. The attitude matrix for the transformation between the

inertial and body reference frames, using a 3-2-1 rotation is [18]

$$A_{BI} = \begin{bmatrix} \cos\phi\cos\theta & \sin\phi\cos\theta & -\sin\theta \\ -\sin\phi\cos\psi + \cos\phi\sin\theta\sin\psi & \cos\phi\cos\psi + \sin\phi\sin\theta\sin\psi & \cos\theta\sin\psi \\ \sin\phi\sin\psi + \cos\phi\sin\theta\cos\psi & -\cos\phi\sin\psi + \sin\phi\sin\theta\cos\psi & \cos\theta\cos\psi \end{bmatrix} \tag{3.31}$$

The kinematic relation for Equation 3.31 is $B(\theta, \psi)$ where ϕ is yaw, θ is roll, and ψ is pitch.

$$\begin{bmatrix} \dot{\phi} \\ \dot{\theta} \\ \dot{\psi} \end{bmatrix} = B(\theta, \psi)\vec{\omega} \tag{3.32}$$

The angular velocities about their respective axes are represented as $\vec{\omega} \equiv [\omega_1\ \omega_2\ \omega_3]^T$. These dynamics are rewritten as:

$$\begin{bmatrix} \dot{\phi} \\ \dot{\theta} \\ \dot{\psi} \end{bmatrix} = \frac{1}{\cos\theta} \begin{bmatrix} 0 & \sin\psi & \cos\psi \\ 0 & \cos\theta\cos\psi & -\cos\theta\sin\psi \\ \cos\theta & \sin\theta\sin\psi & \sin\theta\cos\psi \end{bmatrix} \begin{bmatrix} \omega_1 \\ \omega_2 \\ \omega_3 \end{bmatrix} \tag{3.33}$$

so $\cos(\theta) \neq 0$. When θ equals $\pm\frac{\pi}{2}$ radians, a singularity occurs. The physical configuration of the ACSPG prevents pitch and yaw rotation exceeding $\frac{pi}{6}$ radians.

The angular momentum of a body $\vec{H}$ with respect to the origin of the inertial coordinate system is

$$\vec{H}^0 = \sum_{i=1}^{n} \vec{r}^{\,i0} \times m_i \vec{v}^{\,i0} \tag{3.34}$$

where i represents all of the point masses comprising the body.

To use the angular momentum of the COM in the body frame requires a transformation from the inertial frame as presented in Equation (2.4) to the body

frame and is given by

$$\vec{H}_B^c = A_{BI}\vec{H}_I^C = A_{BI}\bar{J}_I^C\vec{\omega}_I^{BI} = \bar{J}_B^C\vec{\omega}_B^{BI} \tag{3.35}$$

The inverse follows such

$$\vec{\omega}_B^{BI} = (\bar{J}_B^c)^{-1}\vec{H}_B^c \tag{3.36}$$

as long as each rotation is about a principal axis, the angular momentum and angular velocity of the body remain parallel [18] The first derivative of angular momentum is torque.

$$\frac{d\vec{H}}{dt} = \dot{\vec{H}} = \vec{L} \tag{3.37}$$

when the COM is not at the COR, this can is rewritten as

$$\frac{dH_0}{dt} = (\vec{r} \times m\ddot{\vec{r}}) + \dot{H}_c + [\vec{\omega} \times (\vec{r} \times m\dot{\vec{r}})] + (\vec{\omega} \times \vec{H}_c) \tag{3.38}$$

which reduces to

$$\dot{\vec{H}}_B^C = \vec{L}_B^C - \vec{\omega}_B^{BI} \times \vec{H}_B^C \tag{3.39}$$

combining with Equation 3.35

$$\dot{\vec{\omega}}_B^{BI} = (\bar{J}_B^C)^{-1}[\vec{L}_B^C - \vec{\omega}_B^{BI} \times (\bar{J}_B^C\vec{\omega}_B^{BI})] \tag{3.40}$$

Assuming the motion and off-axis terms are small compared to the other terms, $\dot{\vec{\omega}}$ simplifies to

$$\dot{\vec{\omega}} = \begin{bmatrix} \frac{mg}{J_{xx}}(-r_y \cos\psi \cos\theta + r_z \sin\psi \cos\theta) \\ \frac{mg}{J_{yy}}(r_x \cos\psi \cos\theta + r_z \sin\theta) \\ \frac{mg}{J_{zz}}(-r_x \sin\psi \cos\theta + r_y \sin\theta) \end{bmatrix} \tag{3.41}$$

where $J_{xx,yy,zz}$ are the MOIs about each axis.

The angular accelerations are integrated:

$$\int \dot{\vec{\omega}} = mg \begin{bmatrix} \int(-r_y \cos\psi \cos\theta + r_z \sin\psi \cos\theta)/J_{xx} \\ \int(r_x \cos\psi \cos\theta + r_z \sin\theta)/J_{yy} \\ \int(-r_x \sin\psi \cos\theta + r_y \sin\theta)/J_{zz} \end{bmatrix} \tag{3.42}$$

producing

$$\vec{\omega}_{x_{t2}} - \vec{\omega}_{x_{t1}} = \frac{mg\Delta t}{2J_{xx}} \left[\left((\cos\phi \cos\theta)_{t2} + (\cos\phi \cos\theta)_{t1} \right) r_y - \left((\sin\phi \cos\theta)_{t2} + (\sin\phi \cos\theta)_{t1} \right) r_z \right] \tag{3.43}$$

$$\vec{\omega}_{y_{t2}} - \vec{\omega}_{y_{t1}} = \frac{mg\Delta t}{2J_{yy}} \left[\left((\cos\phi \cos\theta)_{t2} + (\cos\phi \cos\theta)_{t1} \right) r_x + \left((\sin\theta)_{t2} + (\sin\theta)_{t1} \right) r_z \right] \tag{3.44}$$

$$\vec{\omega}_{z_{t2}} - \vec{\omega}_{z_{t1}} = \frac{mg\Delta t}{2J_{zz}} \left[\left((\sin\phi \cos\theta)_{t2} + (\sin\phi \cos\theta)_{t1} \right) r_x + \left((\sin\theta)_{t2} + (\sin\theta)_{t1} \right) r_y \right] \tag{3.45}$$

where t_1 represents values at the first time step and t_2 represents values at the second time step. This is written in matrix form as:

$$\begin{pmatrix} \Delta\omega_x \\ \Delta\omega_y \\ \Delta\omega_z \end{pmatrix} = \frac{mg\Delta t}{2} \begin{bmatrix} 0 & -\left((c\phi c\theta)_{t2} + (c\phi c\theta)_{t1}\right)/I_{xx} & \left((s\phi c\theta)_{t2} + (s\phi c\theta)_{t1}\right)/I_{xx} \\ \left((c\phi c\theta)_{t2} + (c\phi c\theta)_{t1}\right)/I_{yy} & 0 & \left((s\theta)_{t2} + (s\theta)_{t1}\right)/I_{yy} \\ -\left((s\phi c\theta)_{t2} + (s\phi c\theta)_{t1}\right)/I_{zz} & -\left((s\theta)_{t2} + (s\theta)_{t1}\right)/I_{zz} & 0 \end{bmatrix} \begin{pmatrix} r_x \\ r_y \\ r_z \end{pmatrix} \tag{3.46}$$

where cϕ and sϕ are used to represent cos and sin of each respective angle. Rearranging Equation 3.46 allows for solving for the position vector of the offset between the COM and COR.

3.5 Evaluating the Methods

Both methods require evaluation with several factors. MATLAB is used to perform several simulations. The non-linear control is simulated and verified with varied masses and MOI. This allows for testing the model and tuning it based on the changing variables. The least squares estimation method is tested by adding noise to simulated angular rates and then simulated at varying time intervals to determine the convergence ability of the method.

The most important element is the ability of a method to quickly converge on a solution. While simplifying assumptions ease the development of each method, importance is placed on minimizing assumptions. Assumptions may impact the accuracy of the results, as such weight is given to limiting assumptions.

3.6 Non-orthogonal Equations

Upon determining the relation between the COM and the COR, the desired location of the sliding masses is determined. The initial centroid of the overall system relative to the center of the air bearing, r is

$$r = \frac{1}{M}[(M - \sum_{j=1}^{5} m_j)r_0 + \sum_{j=1}^{5} m_j r_{j,0}] \tag{3.47}$$

where r_0 represents the location of the centroid of the ACSPG without the balancing system, M is the mass of the whole simulator, and $r_{j,0}$ is the initial position of each slider. A top down view of the sliding masses along their actuators in the x-y plane is depicted in Figure 9

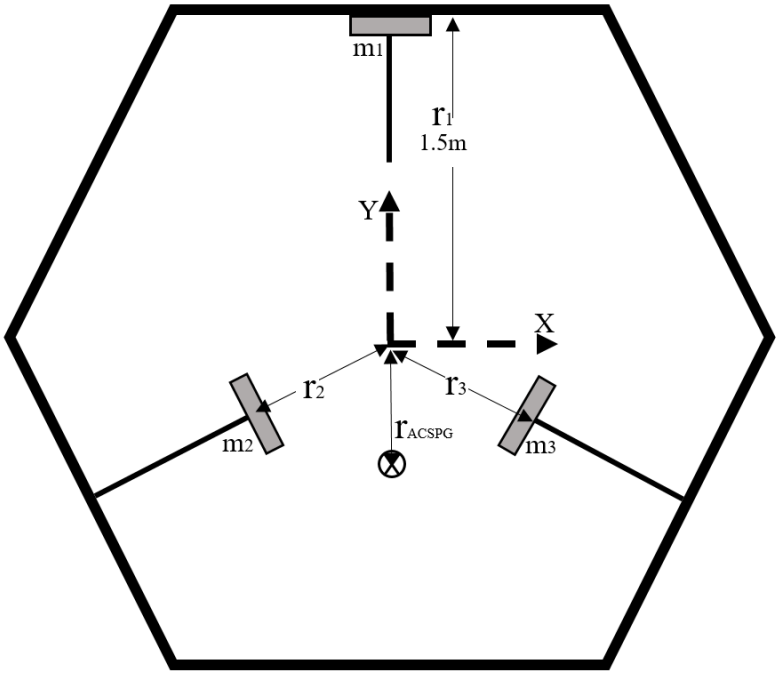

Figure 9. Depiction of sliders in the horizontal plane

As the sliders are moved, the new location of the centroid and sliders are given by

$$r_{new} = \frac{1}{M}[(M - \sum_{j=1}^{5} m_j)r_0 + \sum_{j=1}^{5} m_j r_{j,new}] \tag{3.48}$$

the resulting change in location of the overall system centroid becomes:

$$\Delta r = r_{new} - r = \frac{1}{M}[(M - \sum_{j=1}^{5} m_j)r_0 + \sum_{j=1}^{5} m_j r_{j,new}] - \frac{1}{M}[(M - \sum_{j=1}^{5} m_j)r_0 + \sum_{j=1}^{5} m_j r_{j,0}] \tag{3.49}$$

and this reduces to

$$\Delta r = \frac{1}{M} \sum_{j=1}^{5} m_j \Delta r_j \tag{3.50}$$

For a mass balancing system with orthogonally configured actuators and masses, the motion of the centroid $r_{x,y,z}$ is directly mapped to a sliding moving along each axis. All sliding masses are equivalent in mass. Each Δr is then solved for by

$$\begin{bmatrix} \Delta x \\ \Delta y \\ \Delta z \end{bmatrix} = \frac{M}{m_p} \begin{bmatrix} \Delta r_x \\ \Delta r_y \\ \Delta r_z \end{bmatrix} \tag{3.51}$$

where Δx, Δy, and Δz represent the change in position of a slider corresponding to each axis. However, due to AFRL's non-orthogonal configuration, the positioning of the masses is determined by the following method with changes in the centroid mapped to the five sliding masses. First, the three horizontal sliding masses each have components of motion in the X and Y directions. Their changes in movement are solved by

$$\Delta X = \sum_{j=1}^{3} cos\theta_j \Delta r_j \tag{3.52}$$

$$\Delta Y = \sum_{j=1}^{3} -\sin\theta_j \Delta r_j \tag{3.53}$$

where θ_j represents the known angle between the x-axis and each linear actuator. The positions of the two vertically sliding masses are solved by

$$\Delta Z = \Delta r_4 + \Delta r_5 \tag{3.54}$$

Equations 3.52 - 3.54 are combined with Equation 3.51 and rewritten as

$$\frac{M}{m_p}\begin{bmatrix} \Delta X \\ \Delta Y \\ \Delta Z \end{bmatrix} = \begin{bmatrix} cos\theta_1 & cos\theta_2 & cos\theta_3 & 0 & 0 \\ -\sin\theta_1 & -\sin\theta_2 & -\sin\theta_3 & 0 & 0 \\ 0 & 0 & 0 & 1 & 1 \end{bmatrix} \begin{bmatrix} \Delta r_1 \\ \Delta r_2 \\ \Delta r_3 \\ \Delta r_4 \\ \Delta r_5 \end{bmatrix} \tag{3.55}$$

As this is not a square matrix a pseudoinverse is utilized to rearrange this as follows

$$\begin{bmatrix} \Delta r_1 \\ \Delta r_2 \\ \Delta r_3 \\ \Delta r_4 \\ \Delta r_5 \end{bmatrix} = \frac{M}{m_p} \begin{bmatrix} cos\theta_1 & cos\theta_2 & cos\theta_3 & 0 & 0 \\ -\sin\theta_1 & -\sin\theta_2 & -\sin\theta_3 & 0 & 0 \\ 0 & 0 & 0 & 1 & 1 \end{bmatrix}^{\dagger} \begin{bmatrix} \Delta X \\ \Delta Y \\ \Delta Z \end{bmatrix} \tag{3.56}$$

where '†' is used to notate the required Moore-Penrose pseudoinverse.

3.7 Conclusion

Due to the unique characteristics of the ACSPG, determining the control algorithms for automatically balancing the system was necessary. This was determined via two methods used on other systems and applied to the ACSPG.

Also, a method of mapping changes to the centroid to a non-orthogonal mass balancing configuration was presented. The next chapter is used to test the effectiveness of the methods.

IV. Results and Analysis

4.1 Overview

This chapter applies the methodologies presented in Chapter III to account for and mitigate the gravitational torques as identified in Section 1.4. An iterative approach is used to apply the presented techniques and evaluate their applicability and performance. While developing the models, refining the initial conditions and tuning k_p are also important. All simulations in this research were performed using a Hewlett Packard® computer with a 3.5 GHz Intel ® processor with four cores and 32 Gb of random access memory.

First, this chapter presents the non-linear adaptive control method, detailing the ability of the control to account for both horizontal and vertical offsets. Second, this chapter presents an examination of the recursive least squares approach. Last is a determination of the maximum allowable variation between the COM and COR. This chapter concludes by reviewing the performance of the two balancing methods.

4.2 Non-linear Adaptive Control Method

The application of the aforementioned nonlinear adaptive control requires verifying the performance of the control by ensuring the ability of the control method to produce a constant angular velocity. A constant angular velocity indicates no gravitational torque is present to cause angular acceleration. This is initially done by simulating a system similar to that at NPS. After verification, the next step is to increase the mass and MOI, ultimately to the levels of the ACSPG. The ability of the control method to adequately compensate for greater mass and MOI parameters requires performance within the capabilities of the ACSPG's design.

This control algorithm was initially utilized by NPS on a system with an inertia matrix of $\bar{J} = \text{diag}(0.0226, 0.0257, 0.0266)$ kg $\cdot$ m^2, a simulator mass of $m_{s/c} = 4.2$ kg, and three orthogonally arranged 0.3 kg sliding masses [7]. Furthermore, the system is excited with an initial angular velocity of $\vec{\omega} = [0.0888\ 0.8229\ 1.3611]^T$ rad/s and a simulated offset between the COM and COR of $\vec{r}_{off} = [1\ \ -0.9\ \ -1.4]^T \cdot 10^{-3}$ m. The simulation of the balancing procedure in this research utilizes these conditions as a starting point. This is solved in MATLAB and the time the system requires to reach equilibrium is less than two seconds.

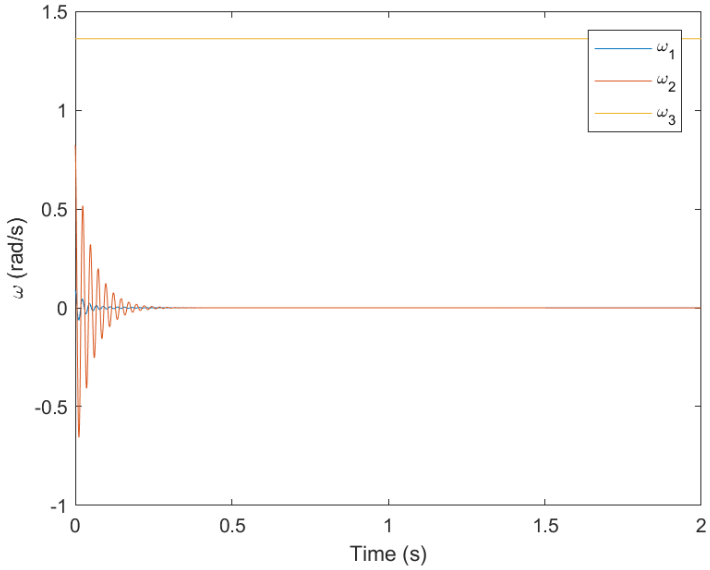

Figure 10. Angular Velocity (rad/s) with a simulator mass of 4.2 kg, slider mass of 0.3 kg, MOI=diag(0.0226; 0.0257; 0.0266) kg m^2, ω_0=[0.0888 0.8229 1.3611]' rad/s, and k_p=1

In Figure 10, the angular velocities of the satellite simulator about the horizontal axes, ω_1 and ω_2, are driven to zero. The angular velocities about the vertical axis, ω_3, remain at their initial value and are not compensated for by the horizontal balancing procedure. The initial angular velocity about axis one is smaller than that about axis two and is compensated much more quickly than the angular velocity about axis two.

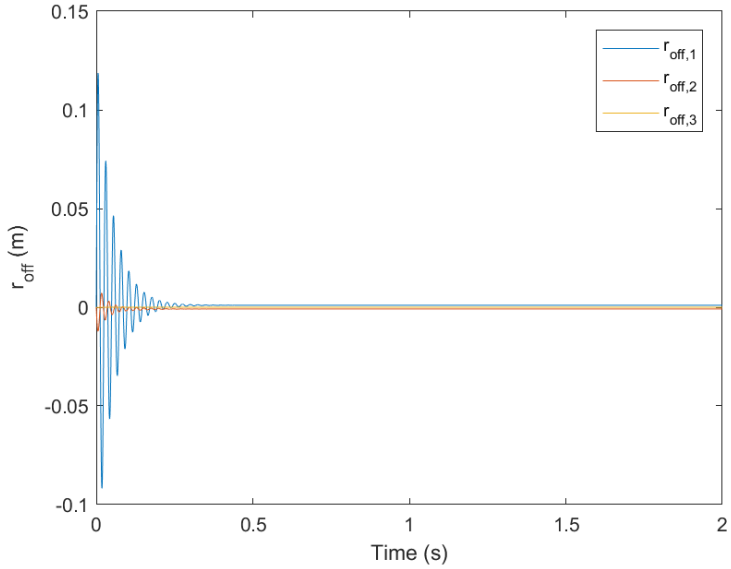

Figure 11. Determination of r_{off} with a simulator mass of 4.2 kg, slider mass of 0.3 kg, MOI=diag(0.0226; 0.0257; 0.0266) kg m^2, ω_0=[0.0888 0.8229 1.3611]' rad/s, and k_p=1

Figure 11 plots the estimated location of the COM relative to the COR. As the system runs, the r_{off} vector is driven to the steady state simulated truth value. This demonstrates an ability to quickly and accurately balance the system.

The error of the estimated position relative to the simulated offset quickly approaches zero as seen in Figure 12. Figure 13 illustrates the change in position of each sliding mass, indicating the necessary actuator length before also reaching a neutral position. The simulation has performed as expected in quickly and accurately estimating the offset while simulating motion of the sliding masses.

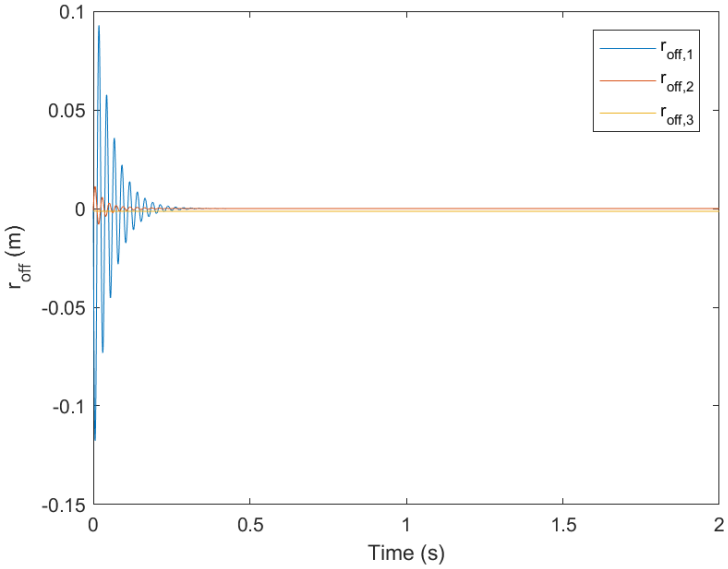

Figure 12. Estimated offset error of the COM displacement with a simulator mass of 4.2 kg, slider mass of 0.3 kg, MOI=diag(0.0226; 0.0257; 0.0266) kg m^2, ω_0=[0.0888 0.8229 1.3611]' rad/s, and k_p=1

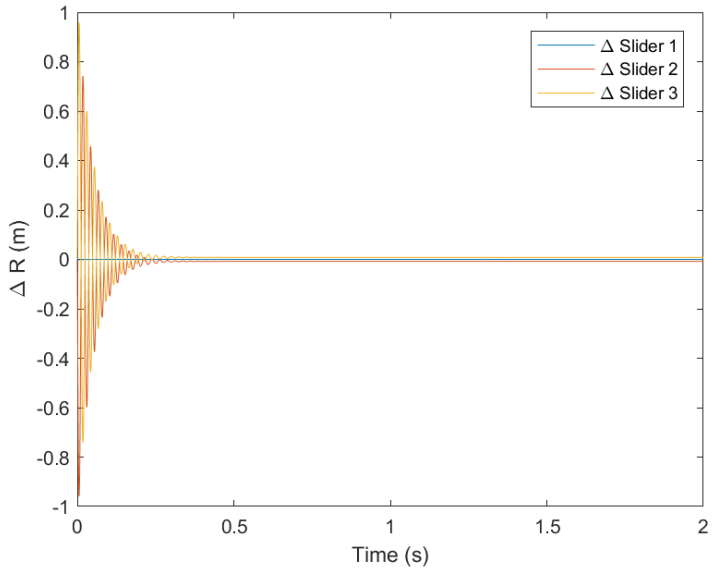

Figure 13. Change in horizontal slider positions with a simulator mass of 4.2 kg, slider mass of 0.3 kg, MOI=diag(0.0226; 0.0257; 0.0266) kg m^2, ω_0=[0.0888 0.8229 1.3611]' rad/s, and k_p=1

4.2.1 Parametric Study

Upon verifying the control capably balances a system similar to that at NPS, it is necessary to increase the mass and MOI properties of the simulated system and test the response. The MOI and the masses of the structure and sliding masses are increased to identify the system response. The simulations are again performed in MATLAB.

The increased mass and MOI values result in longer balancing times and the oscillation frequency and magnitude increases for the mass positions relative to those seen above in Figures 10-13. As is stated in Chapter III k_p is a tunable value. While previously indicated as an arbitrary value, k_p does possess significance in determining an improved solution [7]. Increasing k_p increases the system response and causes the system to balance faster. Full results of these simulations are presented in Appendix A.

4.2.2 Simulating the Dynamics of the ACSPG

Upon showing this method for balancing the platform accomplishes the intended goal of reducing angular velocity to zero and reaching a steady state for the estimation of r_{off} on smaller scales, the method is applied to the full scale dynamics of the ACSPG. As provided by AFRL, $\bar{J} = diag(1100,\ 2100,\ 1050)\text{kg}\cdot\text{m}^2$.

To better simulate the ACSPG, the MOI is assumed to as $\bar{J} = diag(1106,\ 2274,\ 810)\text{kg}\cdot\text{m}^2$. Appendix B presents intermediate results during the tuning process. The intermediate results required significant computational time of over 6,800 seconds, failed to provide solution is anywhere near converging after 200 seconds of simulated run time, and were highly volatile with frequent oscillations of great magnitude. There is nearly $\pm$ 40m of error in the COM displacement, and the sliders require 3 km actuators.

4.2.2.1 Fixed-step Integrator

One attempt to resolve the volatile nature of the simulations involved utilizing a fixed-step integrator. Using a step size of 0.05 seconds simulates a reasonable data refresh rate. Unfortunately, the step size of 0.05 seconds is too large, and the system fails to converge on a steady state. Decreasing the step size attempts to find a balance between the volatility of the system and the convergence time. Through many adjustments the step size, only significantly small step sizes allow for convergence. This simulation run time also requires significant convergence time and is equally volatile as the previous simulations.

4.2.2.2 System Refinement

The applicability of the proposed balancing method necessitates short computational times and short convergence times. Similarly, the motion of the balancing masses must remain within the limits of the designed actuators. Increasing k_p can shorten the necessary computational time, so this is explored further.

Currently, the system is designed with 20 kg sliding masses. Increasing the mass of each slider allows for a greater magnitude of solvable conditions for r_{off}. Larger sliding masses also create greater control torques, allowing for quicker dampening and shorter traveling distances of the masses. Changing the mass of each slider dictates changes to the configuration of the system and requires different linear actuators. Applying these considerations, each sliding mass increases to 50 kg and k_p=1000 producing results found in Appendix B.

This simulation converges at a much more quickly; however, the travel of the sliding masses is still impractical. Increasing the mass of each sliding mass substantially reduces the distance each slider travels. However, having the masses

travel 1.2 km is highly impractical. There exists a means of applying the balancing system while staying within the limitations of the designed linear actuators.

The initial angular rates and simulated offsets up through this point are those as simulated by NPS [7]. Upon further consideration, exciting a simulator the size of the ACSPG with the large angular rate is impractical. Such initial angular rates are greater than what the ACSPG encounters. The offset between the COR and COM causes an initial rotation immediately after releasing the ACSPG from a level position. The resulting angular velocities are simulated with $\vec{\omega}_0$=[0.4440, 4.1145, 6.8055]$\times 10^{-5}$ and adjusting the tunable constant as k_p=4000 due to the sensitivity of the ACSPG to initial conditions. These changes to the initial conditions produce the following results.

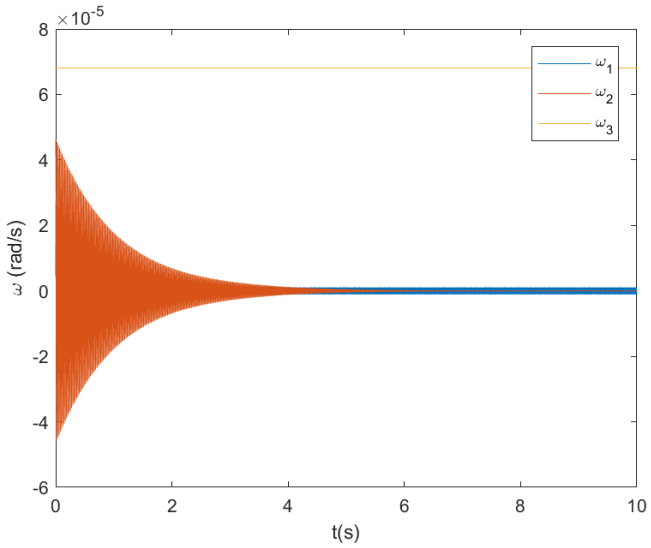

Figure 14. Angular Velocity (rad/s) with a simulator mass of 1375 kg, slider mass of 20 kg, MOI=diag(1100; 2100; 1050) kg m^2, ω_0=$10^{-5}\times$[0.4440, 4.1145, 6.8055]' rad/s, and k_p=4000

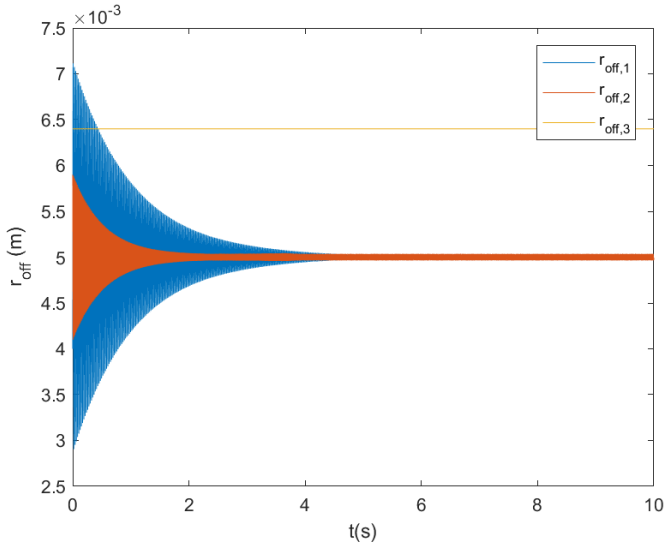

Figure 15. Determination of r_{off} with a simulator mass of 1375 kg, slider mass of 20 kg, MOI=diag(1100; 2100; 1050) kg m^2, ω_0=$10^{-5}\times$[0.4440, 4.1145, 6.8055]' rad/s, and k_p=4000

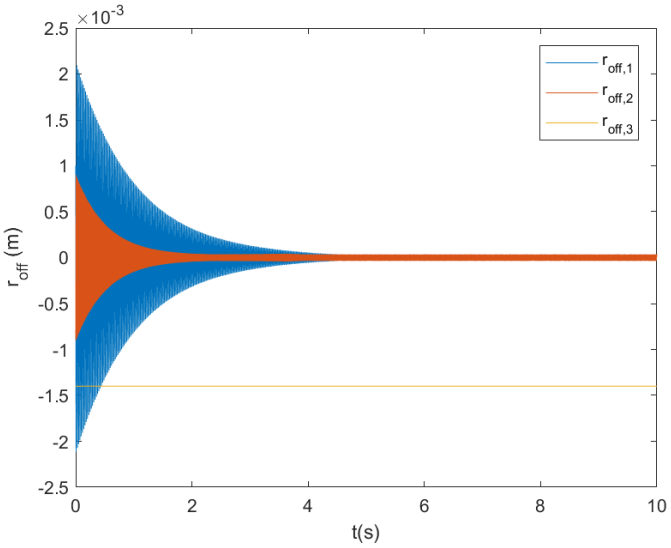

Figure 16. Estimated offset error of COM displacement with a simulator mass of 1375 kg, slider mass of 20 kg, MOI=diag(1100; 2100; 1050) kg m^2, ω_0=$10^{-5}\times$[0.4440, 4.1145, 6.8055]' rad/s, and k_p=4000

Figure 14 illustrates the small initial angular rates. The rates about the two horizontal axes approach steady state within 10 seconds. As seen previously, the

angular rates about the third, vertical axis are uncompensated. This improved system similarly determines the horizontal COM offset in Figure 15, converging in under 10 seconds. The small values of the COM are within the physical volume of the ACSPG. The limits of the deviation of the COM are explored later in this research.

Figure 16 depicts the error between estimated value for r_{off} and the true value. The error of the estimation for axes one and two converges on zero. The offset in the vertical direction is uncompensated, and so the error remains constant and does not converge to zero. Figure 17 demonstrates appropriately constrained motion of

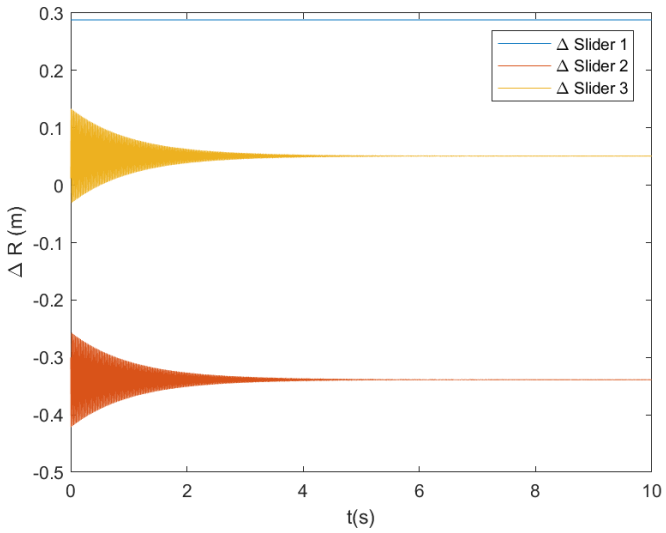

Figure 17. Change in horizontal slider positions with a simulator mass of 1375 kg, slider mass of 20 kg, MOI=diag(1100; 2100; 1050) kg m^2, ω_0=10^{-5}×[0.4440, 4.1145, 6.8055]' rad/s, and k_p=4000

the three horizontal sliding masses. The motion of the sliding masses is restricted to the length of the actuators designed for use on the ACSPG. The system would require further tuning if the motion exceeded 0.6 m.

The tuning parameter k_p was identified previously to affect convergence time. As seen in Figure 18, small values of k_p result in large convergence times, where

larger values of k_p generate shorter convergence times. Tuning k_p can also affect the highly oscillatory nature displayed in the results.

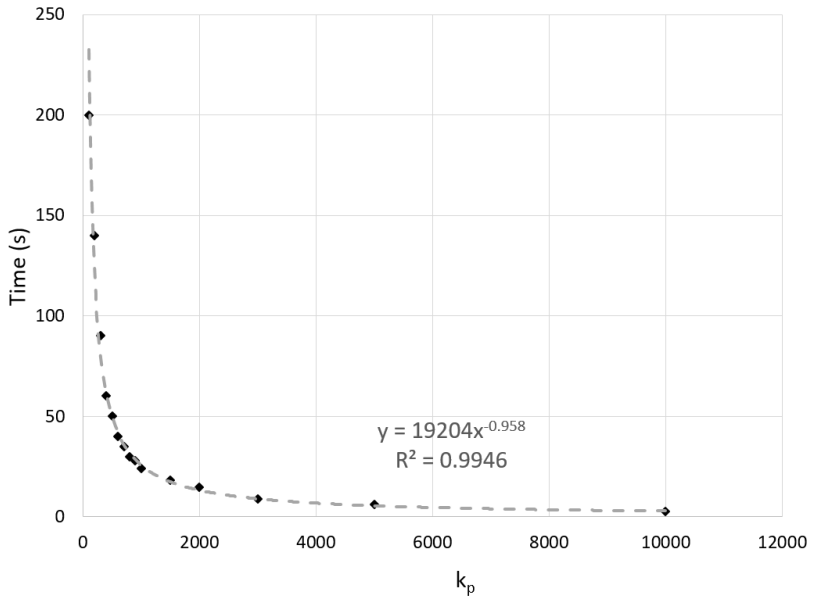

Figure 18. The affects of the tuning parameter k_p on convergence times

4.2.3 Vertical Balancing

The previous section demonstrates successful mitigation of distance between the COR and COM in the horizontal plane. Accounting for vertical offsets is necessary. Offsets in the horizontal plane are perpendicular to the gravitational field, directly correlating to noticeable rotation and tilting of the simulator. Offsets in the vertical direction may still exist, but due to their alignment with the gravitational field, they will not cause rotation to a level platform. Applying the UKF as mentioned in Section 3.3.3 estimates the offsets.

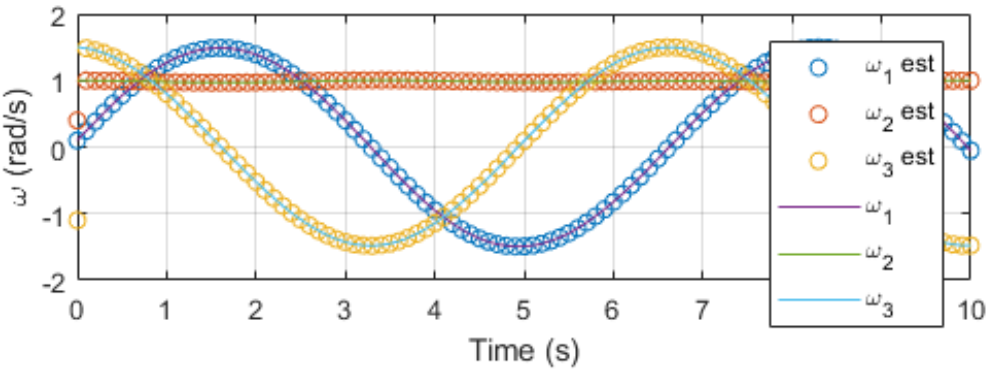

(a)

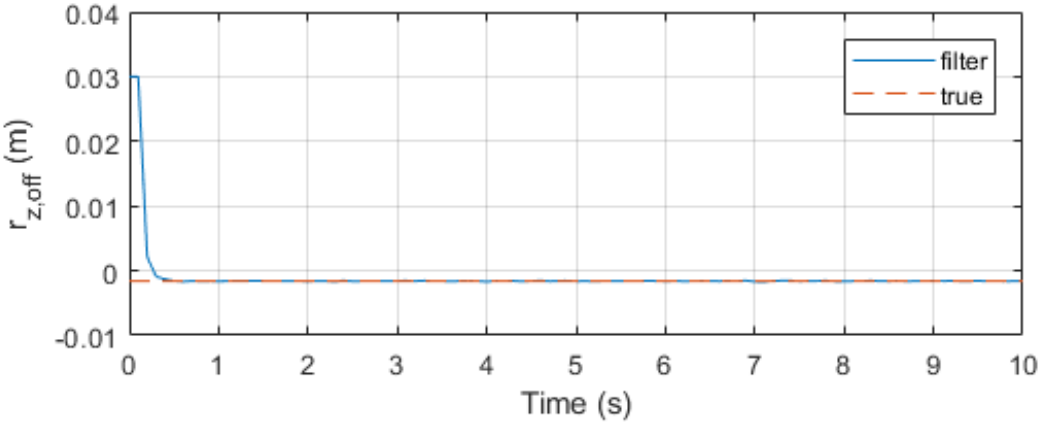

(b)

Figure 19. Estimated (a) angular velocities and (b) r_{off} compared with the simulated true value

Figure 19 illustrates the ability of the filter to quickly and accurately estimate the offset. Even with random noise introduced to the system, the filter maintains small angular rates within the true values as seen in Figure 20. Combining the horizontal nonlinear control method with the vertical offset estimation method, this procedure quickly and effectively determines and adjusts for offsets of the COM relative to the COR.

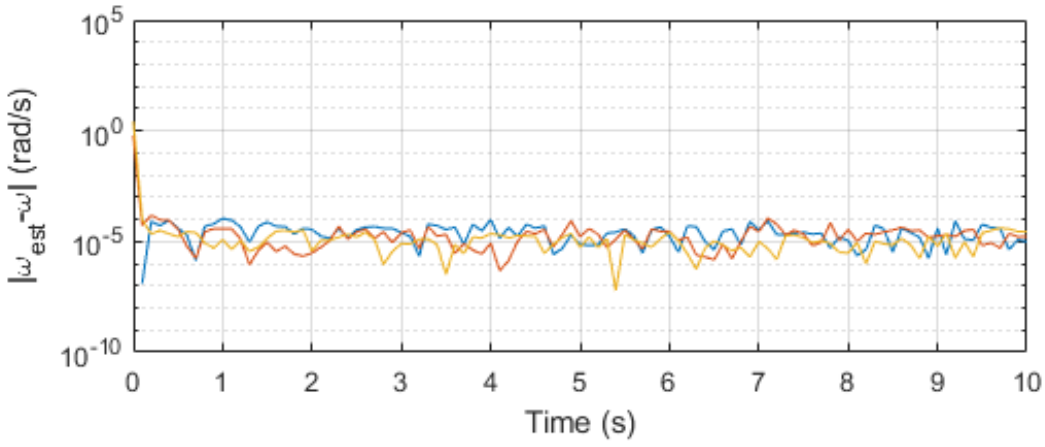

(a)

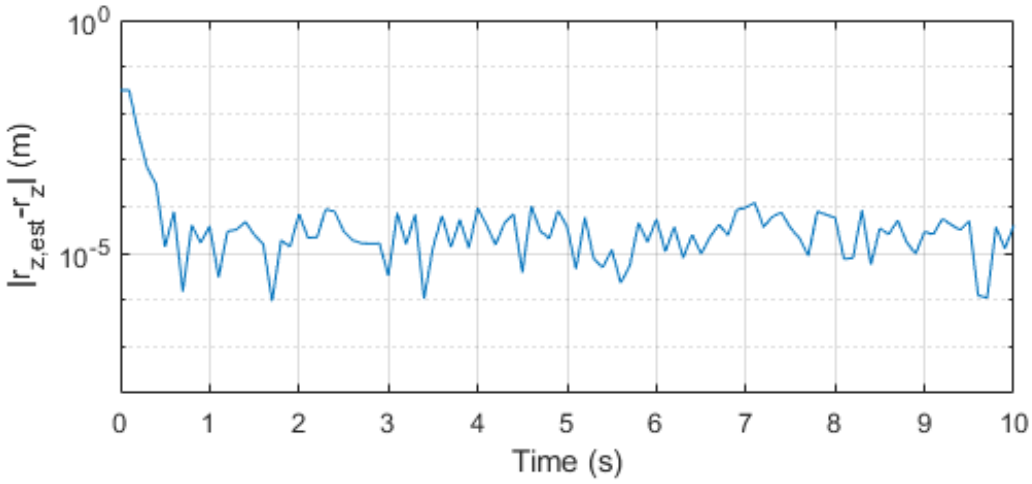

(b)

Figure 20. Error between true and estimated (a) angular velocities and (b) r_{off}

4.3 Recursive Least Squares

Verifying the recursive lease squares approach requires simulating the effectiveness of the method. Upon initial testing of the algorithm, there were consistent errors of 200% between the MATLAB generated data and simulated true values. The error was consistently the same magnitude, but of the opposite sign

from the simulated truth data. This indicates an error in the algorithm as presented by HIT [1].

Revisiting the derivation and making several adjustments ensures consistency with all signs. Upon the next simulation, the system correctly identifies the offset in accordance with the true values. When the presented angular rates are without noise, they converge quickly and precisely.

To increase the realism to the simulation, white Gaussian noise is included. Using an initial angular velocity of $\omega_0 = [0.7,\ 0.5,\ 0.6]$ deg/s, a simulation conducted over an intervals of 30 seconds is presented in Table 1. The estimated offset of the COM relative to the COR is given in the second column. The percentage of error between the truth data and the estimated data is provided in the third column. After a simulation of 30 seconds, all errors are within 2%. The variation of the angular rates are presented in Figures 21.

Table 1. Least Squares Approximation (30 sec.)

	True	Least Squares Estimation	Error
r_x	7.0×10^{-4}	7.075×10^{-4}	1.07654 %
r_y	7.0×10^{-4}	7.129×10^{-4}	1.84765 %
r_z	4.0×10^{-4}	4.071×10^{-4}	1.77566 %

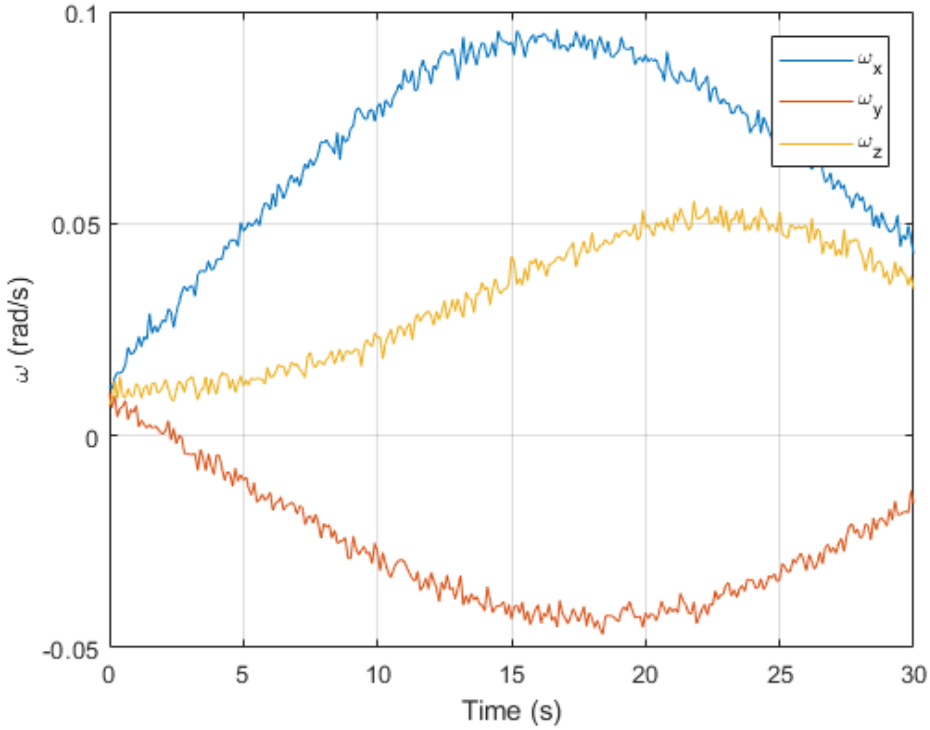

Figure 21. Simulated angular velocity values for 30 seconds

This method is then simulated for 90 seconds produces the following results. The estimated values for r_x, r_y, and r_z are even closer as indicated by the percentage of error in the third column of Table 2. All error values are under 0.5%. The simulated angular velocities with the added noise are depicted in 22. These values are what are integrated according to the equations as presented in Chapter III.

Table 2. Least Squares Approximation (90 sec.)

	True	Least Squares Estimation	Error
r_x	7.0×10^{-4}	6.976×10^{-4}	0.34796 %
r_y	7.0×10^{-4}	6.981×10^{-4}	0.27856 %
r_z	4.0×10^{-4}	4.002×10^{-4}	0.04247 %

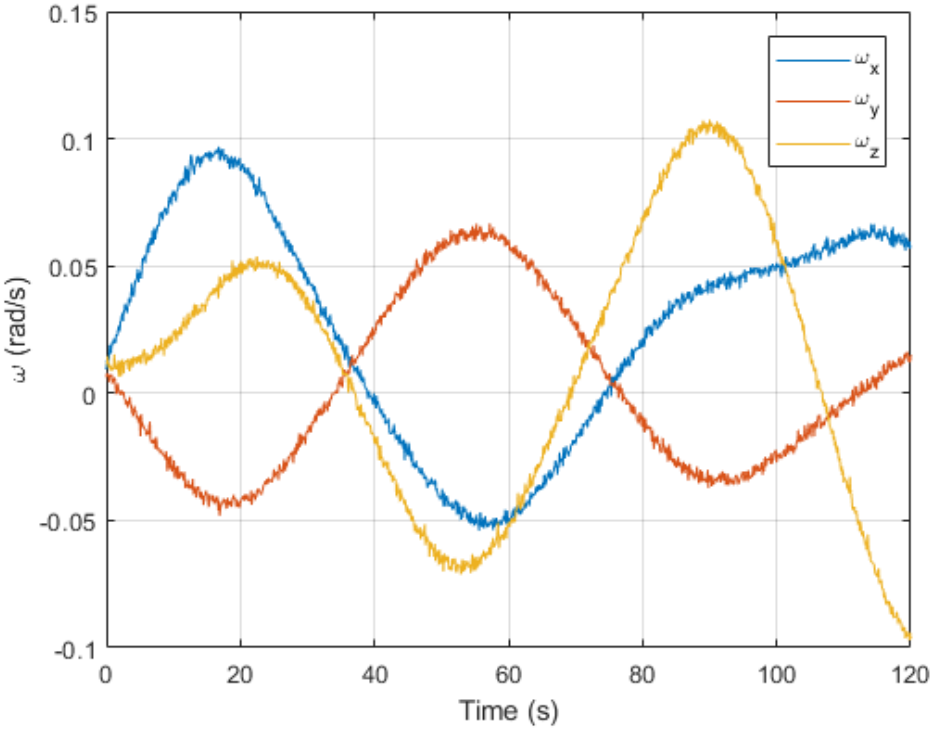

Figure 22. Simulated Euler angles for 120 seconds

The low error values presented in Tables 1 and 2 indicate the least squares method determines the offset within short periods of time. During actual usage of the ACSPG, the collected data is processed and filtered, allowing for more accurate estimations of r_{off}. As presented, the methodology utilizes Euler angles instead of quaternions. The potential remains to re-derive the least squares method using quaternions to prevent any singularities in the attitude information. However, due to the limited time elapsed and the physical limitations of the system, no singularities are expected.

Upon solving for the offset between the COM and COR, the required position of the sliders is easily determined. This method does not eliminate angular velocity, indicating a balanced platform, like the first approach. Upon moving the sliders to the determined locations, no gravitational torques will exist, preventing further

acceleration. As a result, the platform requires leveling before starting any experiments. While similar to the method used at HIT, this model is a vast improvement as it properly accounts for all signs and produces errors less than 0.5%.

4.4 Determining the Performance Envelope

The deviation between the COM and the COR must exist within a small area. The area is limited by the maximum and minimum throw distances of the actuators and the mass of each slider. The small allowable deviations are indicated in Figure 23, where the origin of the plot coincides with the COR. These were determined by using all possible combinations of the sliding mass positions and solving for the given maximum location of the COM given those sliding mass locations.

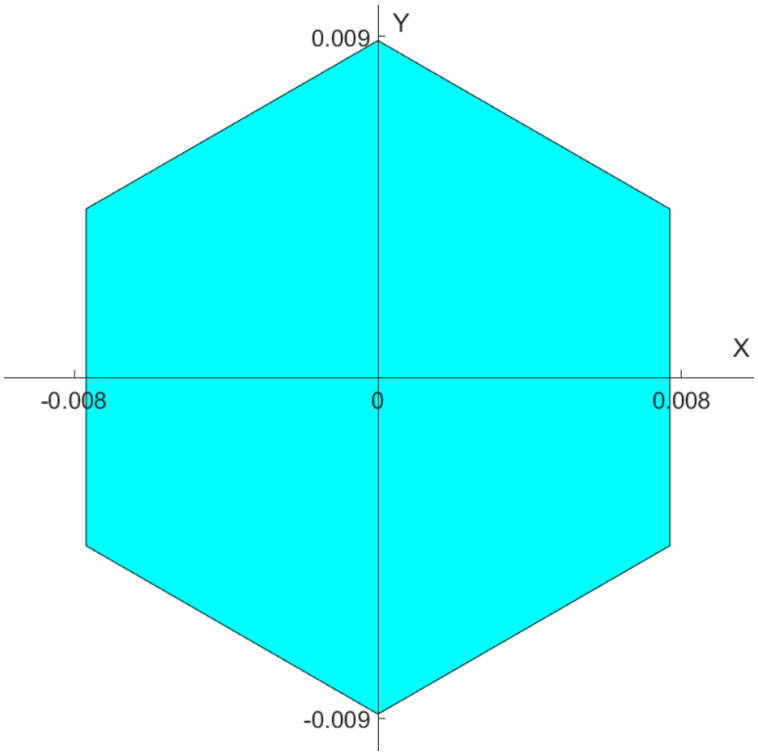

Figure 23. Region of effective COM values in meters

As long as the deviations are within this prescribed area, the balancing system will account for and negate the offset. If the offset is beyond this area, the system is unable to converge upon a solution. To correct for this, the coarse balancing method requires further adjustment until the COM is within the illustrated region.

As was determined while refining the model, there are limitations to the maximum initial angular velocity on the platform. If the initial angular velocity is within that maximum, the control is able to provide a realistic solution. If the initial angular velocity exceeds the maximum value, the control requires motion of the sliding masses beyond the physical limitations of the linear actuators. Using the nine points indicated in Figure 24, the maximum possible initial conditions for angular velocity were determined. Angular velocities were varied about both horizontal axes, and the simulated motion of each sliding mass was analyzed.

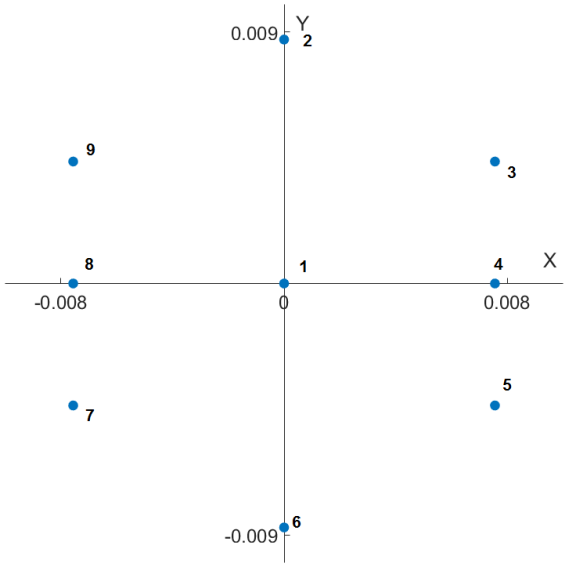

Figure 24. Locations where maximum initial angular velocities were evaluated

The linear actuators have a maximum throw distance of 0.6 meters. During the simulation, if the calculated travel of the sliding mass exceeded this 0.6 meter limit, the angular velocity is determined as unreasonable for the design of the system. The

motion of the non-orthogonal sliding masses is coupled. Because of this, there is not a specific a maximum angular velocity about both axes. The maximum angular velocity about the x-axis exists when the angular velocity of the y-axis is zero and the reverse is also true.

Maximum and minimum throw distances are determined by simulating a range of initial angular velocities about each axis. A difference of less than 0.6 meters between the maximum and minimum throw distance for each sliding mass is required. If the magnitude of the mass travel is within the 0.6 meter limitation a potential initial condition is indicated. Using $\omega_0 \leq [9.0; 8.0; 0] \times 10^{-5}$ rad/s produces a difference between the maximum and minimum change of position for each sliding mass of less than 0.6 meters at each of the nine points. While there are possible combinations where one angular velocity is larger and the other smaller than these values, using this ω_0 as a boundary ensures a solvable solution where the motion of the sliding masses is within the limitations of the actuators.

Many combinations of initial angular rates exist which will provide converging solutions within the limitations of the ACSPG's design. When looking at the identified 9 extreme points, Table 3 depicts maximum initial angular velocities about the x-axis when the angular velocity about the y-axis is zero. Similarly, Table 4 depicts maximum initial angular velocities about the y-axis when the angular velocity about the x-axis is zero for those same 9 points. Any initial excitation greater than these tabulated values requires a solution not possible with the current design of the ACSPG.

4.5 Summary

This chapter investigated two different balancing methods. The non-linear control method required significant refinement to the simulated initial conditions to

Table 3. Tabulated values for the maximum initial angular velocity about the x-axis at varried COM offsets

Point	$r_{off,x}$ (m)	$r_{off,y}$ (m)	$\omega_x(rad/s)$	$\omega_y(rad/s)$
1	0	0	1.99×10^{-4}	0
2	0	8.73×10^{-3}	1.32×10^{-4}	0
3	7.56×10^{-3}	4.36×10^{-3}	1.99×10^{-4}	0
4	7.56×10^{-3}	0	1.99×10^{-4}	0
5	7.56×10^{-3}	-4.36×10^{-3}	1.99×10^{-4}	0
6	0	-8.73×10^{-3}	1.30×10^{-4}	0
7	-7.56×10^{-3}	-4.36×10^{-3}	1.99×10^{-4}	0
8	-7.56×10^{-3}	0	1.99×10^{-4}	0
9	-7.56×10^{-3}	4.36×10^{-3}	1.99×10^{-4}	0

Table 4. Tabulated values for the maximum initial angular velocity about the y-axis at varried COM offsets

Point	$r_{off,x}$ (m)	$r_{off,y}$ (m)	$\omega_x(rad/s)$	$\omega_y(rad/s)$
1	0	0	0	1.56×10^{-4}
2	0	8.73×10^{-3}	0	1.56×10^{-4}
3	7.56×10^{-3}	4.36×10^{-3}	0	1.07×10^{-4}
4	7.56×10^{-3}	0	0	1.56×10^{-4}
5	7.56×10^{-3}	-4.36×10^{-3}	0	9.90×10^{-5}
6	0	-8.73×10^{-3}	0	1.56×10^{-4}
7	-7.56×10^{-3}	-4.36×10^{-3}	0	1.02×10^{-4}
8	-7.56×10^{-3}	0	0	1.56×10^{-4}
9	-7.56×10^{-3}	4.36×10^{-3}	0	9.90×10^{-5}

allow it to work. The nonlinear control method operates under the assumption of a constant MOI of the platform. Through considerable tuning, the nonlinear control was shown to quickly and effectively minimize angular velocities within the system. The second method, involving a recursive least squares estimating procedure, determines the position of the COM relative to the COR, from which the position of the sliding masses are mapped. The recursive least square method does not level the platform and requires this additional step of moving the masses.

V. Conclusions and Recommendations

The ACSPG is currently balanced via a time consuming and imprecise manual method. This necessitated an automated system to balance the system. This research reviewed two techniques in use on other simulators and detailed the ability to apply such methods to the non-orthogonal configuration of the ACSPG. Application of both methods to the ACSPG is possible within the assumptions and limitations described in this research.

This research improves on the previously presented methods by determining and refining the initial conditions applicable to the ACSPG. Without determining the performance envelope of the ACSPG it is not possible to effectively apply the nonlinear adaptive control. Furthermore, the least squares estimation method as presented in this research identified and corrected an error as presented in the reviewed literature, allowing for effective application to the ACSPG.

5.1 Summarization of Adaptive Nonlinear Control

The first method evaluated in this research employs a nonlinear control to determine the offset between the COM and COR. Sliding masses are adjusted and balance the system, eliminating angular velocities. This method is potentially computationally expensive depending on the initial conditions. It also operates under the assumption the motion of the sliding masses is not significant enough to alter the moment of inertia, and so it is assumed $\dot{\bar{J}} = 0$. NPS determined this as valid for smaller simulators, but this requires verification through experimentation with the ACSPG.

During the research process, it was determined that the initial conditions applied to smaller simulators prevented convergence within the design limitations of

the DMBS. The initial condition for angular velocity used at NPS represented an excitation of the simulator that is too large for the ACSPG. The ACSPG requires an initial angular velocity much closer to the natural rotation of the platform. With proper tuning and a small initial angular velocity, the simulation demonstrated the ability of the nonlinear control to determine r_{off} and produce angular velocities that converge to zero.

5.2 Summarization of Least Squares Method

The second technique utilizes a recursive least squares approach. This methodology estimates the offset between the COM and COR. This estimated offset is used to precisely relocate the sliding masses even in their non-orthogonal configuration. Upon mass relocation, the system requires manual re-leveling before the commencement of experimentation.

As simulated, this method was able to estimate the offset between the COM and the COR within 0.5% after 90 seconds. Longer estimation times provide more accurate results. If the duration of the estimation period results in the platform reaching its physical limits, moving the masses to their estimated positions, relevelling the platform, and running the least squares estimation again allows for improving the estimation of r_{off}.

5.3 Performance Envelope

The nonlinear adaptive control is not only limited by the initial angular velocities on the system, there are limitations to the initial offset between the COM and the COR. These limitations are due to the throw distances of the linear actuators. Vertical offsets must exist between $\pm$ 0.0087 m. Offsets in the horizontal plane are constrained by the hexagonal region depicted in Figure 23 with offsets

along the x-axis between ± 0.0076 m and offsets along the axis between ± 0.0087 m. The current design cannot compensate for offsets beyond these limits. Longer actuators allow for greater initial offsets.

5.4 Future Work

Both of the presented techniques require precise knowledge of the simulator's MOI. Without this knowledge, the balancing system is unable to accurately determine the final positions of the sliding masses. It is imperative for AFRL to perform further refinement of their current MOI estimation of the ACSPG.

In order to properly apply the nonlinear adaptive control to the ACSPG, the actuators require characterization. The actuators must quickly and precisely move the masses in accordance with the nonlinear adaptive control. Characterizing the linear actuators determines their ability to quickly and effectively respond to the controller. If the nonlinear adaptive control determines a solution beyond the capabilities of the actuators, further tuning of the system is required.

In the event that experimental verification determine the assumptions are to great, re-deriving the equations of motion for both methodologies will improve their robustness. Including a changing MOI with the non-linear control ensures accounting for the substantial size difference between the ACSPG and smaller simulators. Using quaternions With least squares removes possibilities of singularities.

Finally, to ensure an accurate moment of inertia, the potential exists for using the least squares method iteratively. If the system does not balance with the determined location of the masses, it indicates an inaccurate MOI. As such, there is the potential to use Euler's equation to solve for the MOI.

5.5 Conclusion

The best solution to the challenges at AFRL is to use a hybridized method. Using the recursive least squares approach approximates the offset between the COM and COR. The non-linear control can use this information to properly reconfigure the masses to provide a level final state with the vertical balancing procedure estimating and accounting for offsets along the z-axis. To simplify the system, applying an orthogonal configuration ensures stability along the principle axes of the simulator. Upon refinement of the mass and MOI properties of the ACSPG implementation of an automated mass balancing system will improve the accuracy of the balancing procedure as well as reduce setup times and increase the duration of experimentation. However, it is very difficult to implement any system without more precisely determining the MOI of the simulator.

Appendix A. Parameter study for larger simulators

Upon verifying the control capably balances a system similar to that at NPS, it is necessary to increase the mass and MOI properties of the simulated system and test the response. The MOI increases to $\bar{J} = \text{diag}(7, 8, 4)\text{kg} \cdot \text{m}^2$, $m_{s/c}$= 45 kg, and balancing masses increase to 5 kg. These are arbitrarily larger values to identify the system response to increased dynamics. The simulations are again performed in MATLAB with an initial angular velocity of $\vec{\omega} = [0.0888\ 0.8229\ 1.3611]^T$ and a simulated offset between the COM and COR of $\vec{r}_{off} = [1\ \ -0.9\ \ -1.4]^T \cdot 10^{-3}$ m.

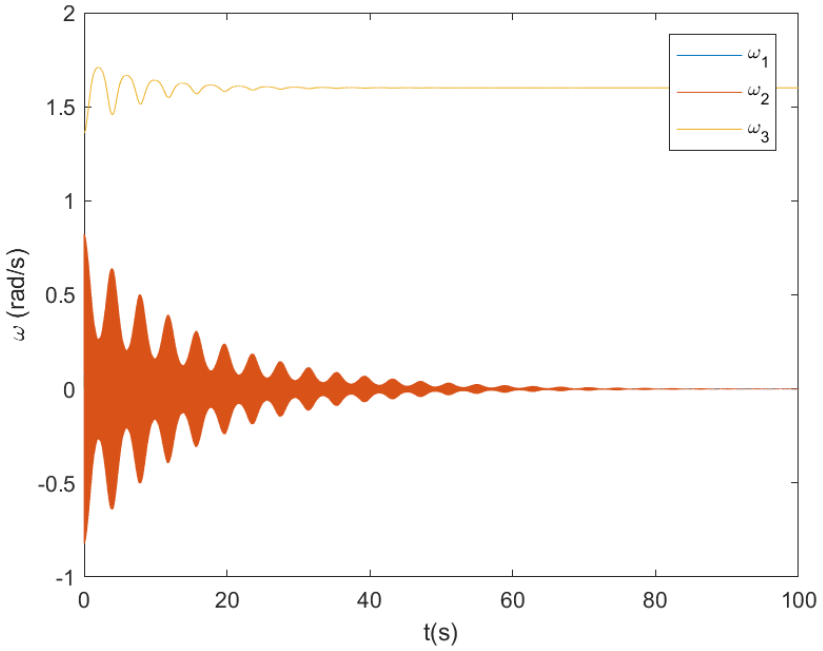

Figure 25. Angular Velocity (rad/s) with a simulator mass of 45 kg, slider mass of 5 kg, MOI=diag(7; 8; 4) kg m^2, ω_0=[0.0888 0.8229 1.3611]' rad/s, and k_p=1

Balancing times are longer and the oscillation frequency for increases for the mass positions relative to those seen above in Figures 10-13. Figure 25 depicts values similar to those seen in Figure 10, albeit oscillating at a much greater rate

and over a longer overall balancing time. The angular velocities about the vertical axis oscillate before settling on the initial, uncompensated initial condition.

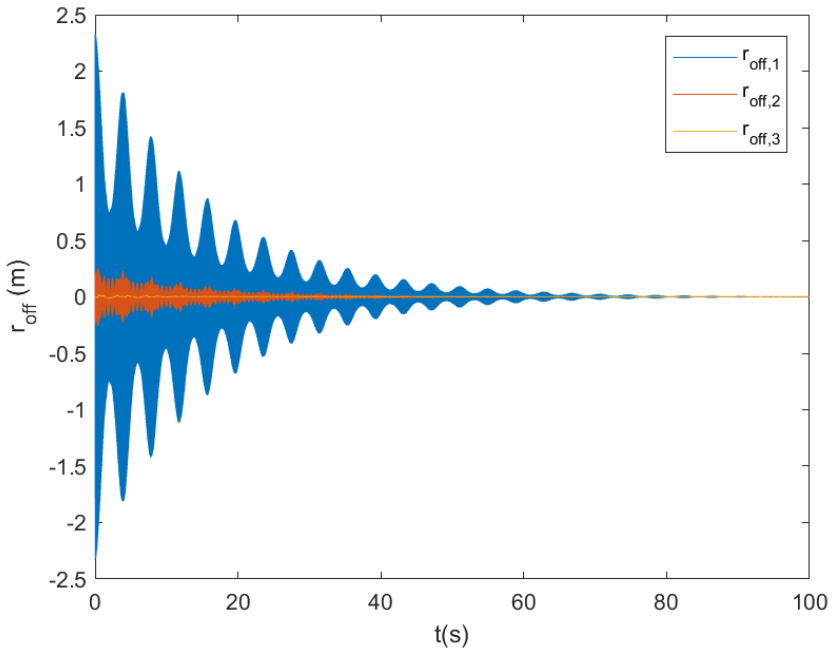

Figure 26. Determination of r_{off} with a simulator mass of 45 kg, slider mass of 5 kg, MOI=diag(7; 8; 4) kg m^2, ω_0=[0.0888 0.8229 1.3611]' rad/s, and k_p=1

The estimation of the COM relative to the COR, r_{off}, in Figure 26 varies between ± 2.5m before ultimate proper determination. An emulator with the above initial conditions would likely have a much smaller diameter than the overall estimation distance of r_{off}, meaning the COM is estimated to travel beyond the physical properties of the simulator.

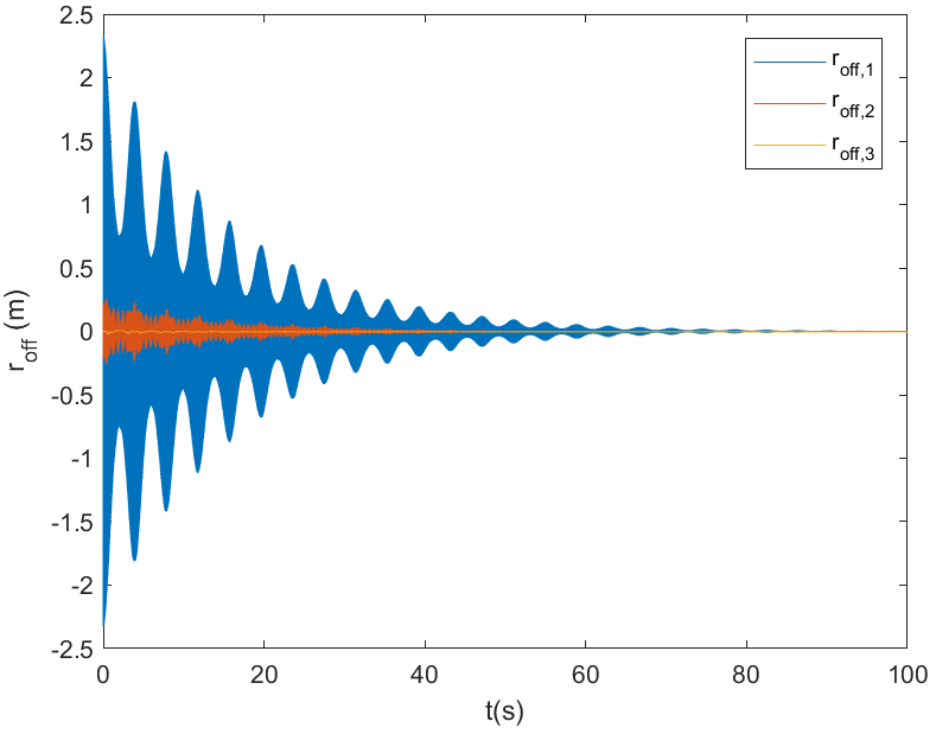

Figure 27. Estimated offset error of COM displacement with a simulator mass of 45 kg, slider mass of 5 kg, MOI=diag(7; 8; 4) kg m^2, ω_0=[0.0888 0.8229 1.3611]' rad/s, and k_p=1

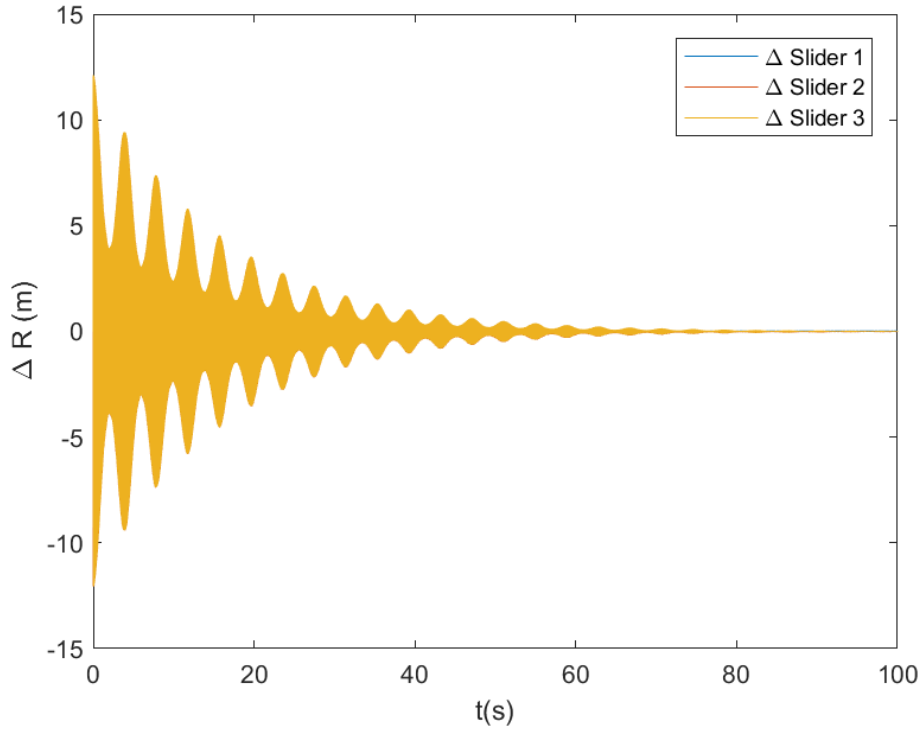

Figure 28. Change in horizontal slider positions with a simulator mass of 45 kg, slider mass of 5 kg, MOI=diag(7; 8; 4) kg m^2, ω_0=[0.0888 0.8229 1.3611]' rad/s, and k_p=1

There is a simulated motion of the sliding masses of more than 12.5 meters in both the positive and negative directions, implying a need of an actuator of approximately 25 meters long. This is unreasonable, and is only exacerbated as the mass and MOI of the platform increase.

As is stated in Chapter III k_p is a tunable value. While previously indicated as an arbitrary value, k_p does possess significance in determining an improved solution [7]. Increasing k_p increases the system response and causes the system to balance faster. The previous simulations used k_p=1, though to see the system response to changing values of k_p, the simulation is rerun with k_p=10.

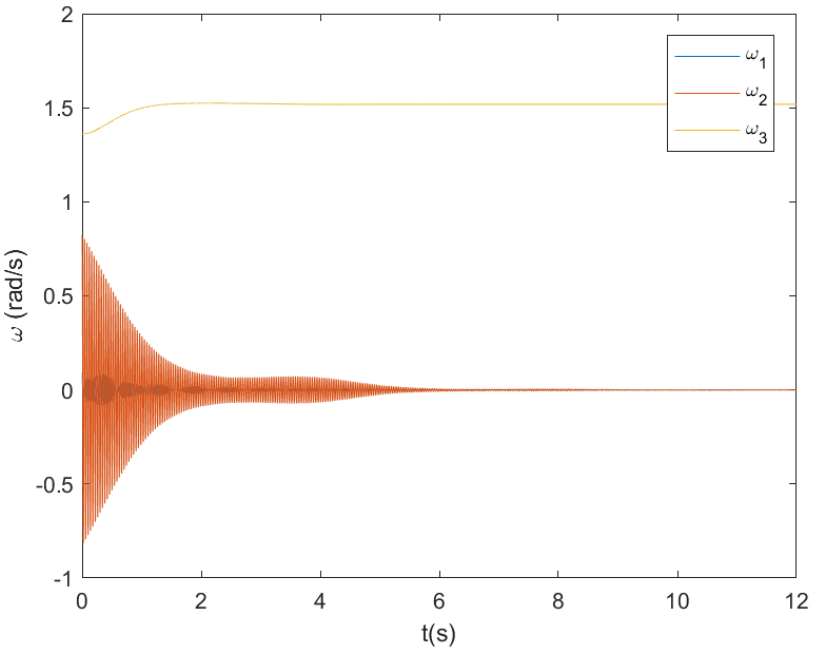

Figure 29. Angular Velocity (rad/s) with a simulator mass of 45 kg, slider mass of 5 kg, MOI=diag(7; 8; 4) kg m^2, ω_0=[0.0888 0.8229 1.3611]' rad/s, and k_p=10

Figure 29 illustrates the effects of increasing k_p on reducing the angular velocity. By increasing k_p from one to 10, the angular velocities about axis one and axis two are reduced to zero in less that one tenth of the time.

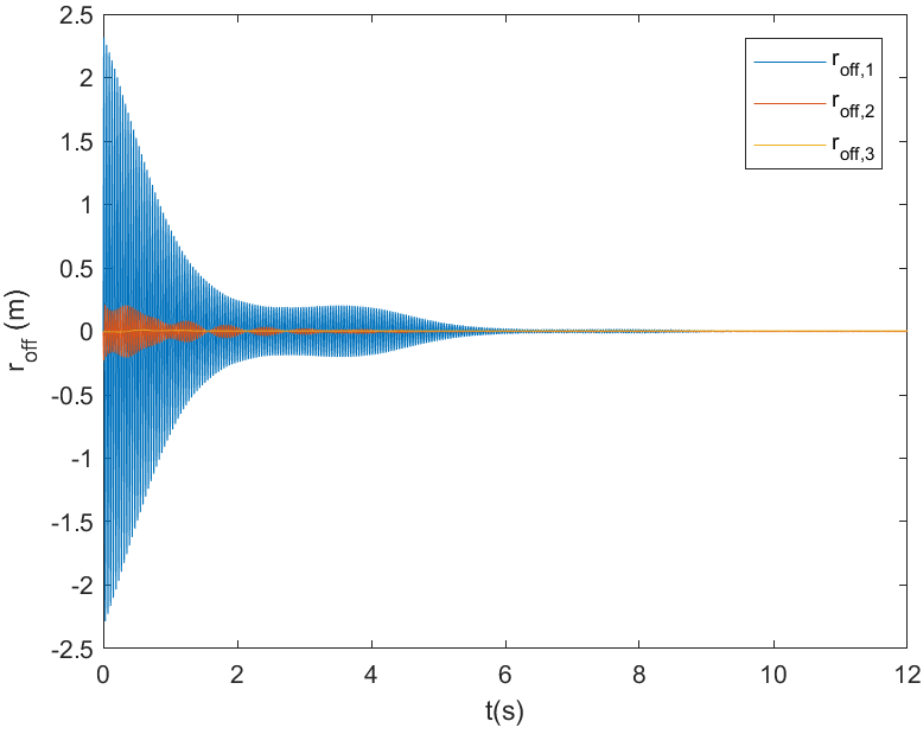

Figure 30. Determination of r_{off} with a simulator mass of 45 kg, slider mass of 5 kg, MOI=diag(7; 8; 4) kg m^2, ω_0=[0.0888 0.8229 1.3611]' rad/s, and k_p=10

Figure 30 has the same initial displacements as Figure 26, indicating the COM is similarly estimated to exist beyond the physical confines of the simulated system. However, it is quickly reduced to small values and reaches a steady state approximation in under 10 seconds.

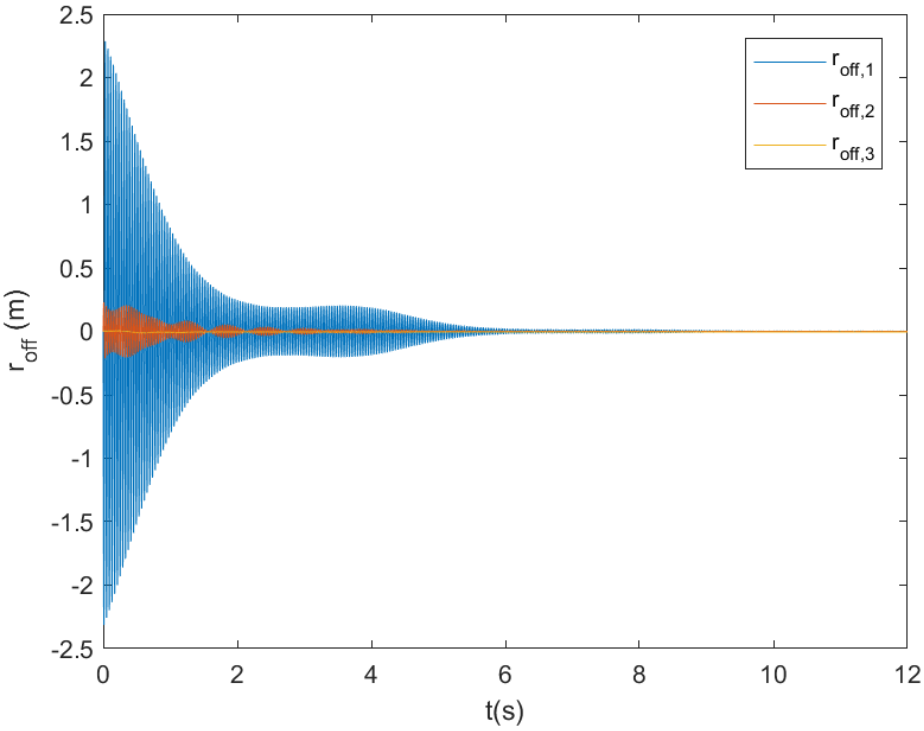

Figure 31. Estimated offset error of COM displacement with a simulator mass of 45 kg, slider mass of 5 kg, MOI=diag(7; 8; 4) kg m^2, ω_0=[0.0888 0.8229 1.3611]' rad/s, and k_p=10

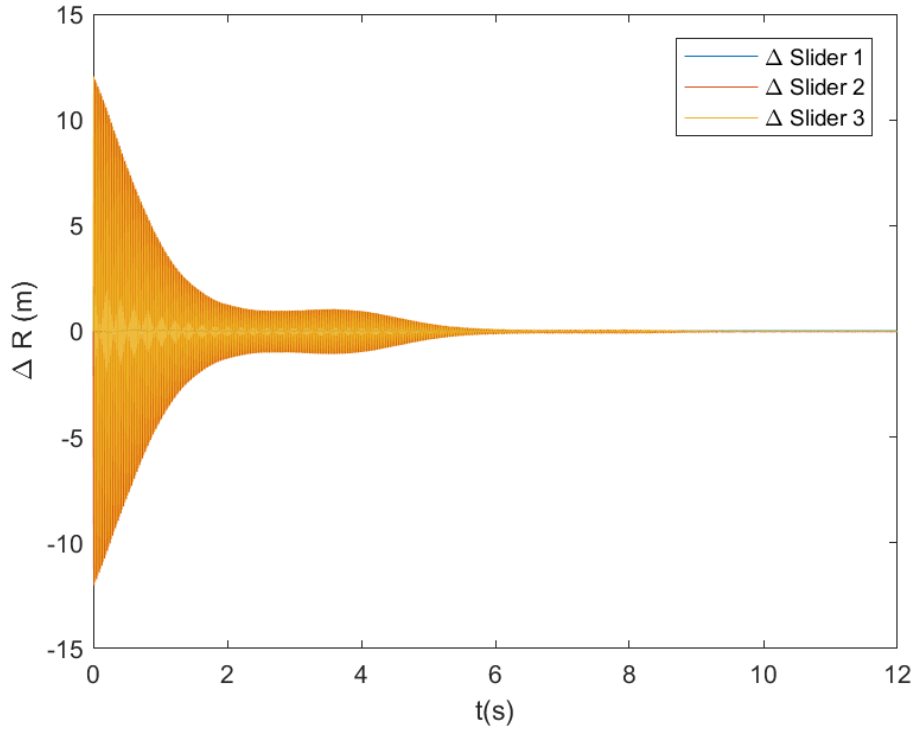

Figure 32. Change in horizontal slider positions with a simulator mass of 45 kg, slider mass of 5 kg, MOI=diag(7; 8; 4) kg m^2, ω_0=[0.0888 0.8229 1.3611]' rad/s, and k_p=10

The two previous plots indicate substantial volatility still exists with the estimation of r_{off}, as indicated by the plot of the estimation error in Figure 31 and the motion of the sliding masses as depicted in Figure 32. However, the system converges much more quickly, both computationally and for the simulated run time of the balancing system to reach a steady state. The motion of the sliding masses along the actuators is still impractical as indicated in Figure 32.

Appendix B. Additional ACSPG Simulations

2.1 Initial Simulations

Upon demonstrating the control system with small masses and MOI, it was necessary to apply it to the ACSPG. AFRL provided an MOI of $\bar{J} = diag(1106,\ 2274,\ 810)\text{kg}\cdot\text{m}^2$. This does not satisfy the triangle inequality.

The triangle inequality requires that for a triangle with sides x, y, and z, the sum of any two sides as greater than the third. For two vectors $\vec{x}$ and $\vec{y}$, summed to equal a third vector $\vec{z}$, $\vec{x} + \vec{y} = \vec{z}$, the following is required as true

$$||\vec{x} + \vec{y}|| \leq ||\vec{x}|| + ||\vec{y}|| \tag{2.1}$$

As such, this research uses an MOI of $\bar{J} = diag(1100,\ 2100,\ 1050)\text{kg}\cdot\text{m}^2$. Figures 33-36, demonstrate highly volatile motion. The system requires significant computational time, over 6800 seconds to determine this solution. Unfortunately, the solution is nowhere near converging after 200 seconds of simulated run time. Figure 35 indicates there is nearly $\pm$ 40m of error in the COM displacement, and the sliders require 3km actuators.

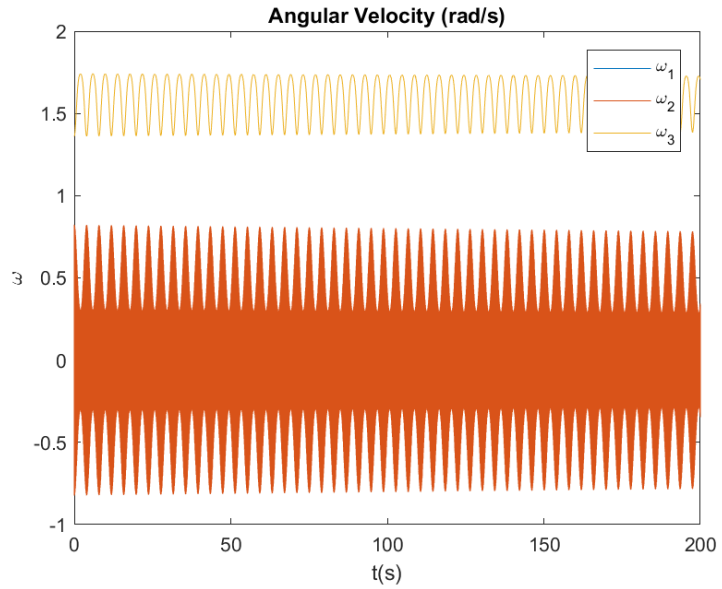

Figure 33. Angular Velocity (rad/s) with a simulator mass of 1375 kg, slider mass of 20 kg, MOI=diag(1100; 2100; 1050) kg m^2, ω_0=[0.0888 0.8229 1.3611]' rad/s, and k_p=1

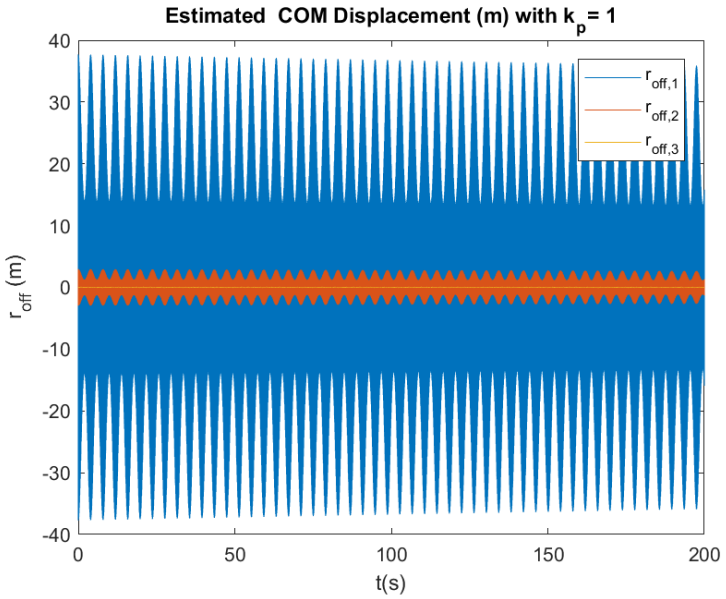

Figure 34. Determination of r_{off} with a simulator mass of 1375 kg, slider mass of 20 kg, MOI=diag(1100; 2100; 1050) kg m^2, ω_0=[0.0888 0.8229 1.3611]' rad/s, and k_p=1

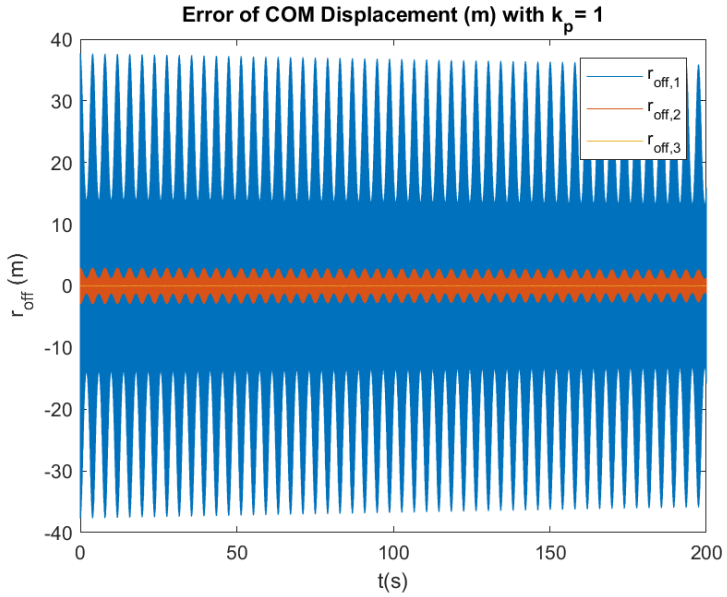

Figure 35. Estimated offset error of COM displacement with a simulator mass of 1375 kg, slider mass of 20 kg, MOI=diag(1100; 2100; 1050) kg m^2, ω_0=[0.0888 0.8229 1.3611]' rad/s, and k_p=1

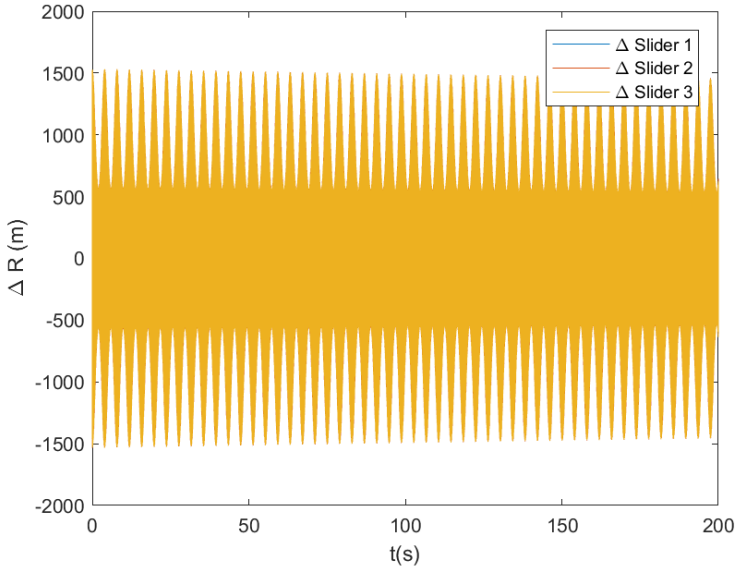

Figure 36. Change in horizontal slider positions with a simulator mass of 1375 kg, slider mass of 20 kg, MOI=diag(1100; 2100; 1050) kg m^2, ω_0=[0.0888 0.8229 1.3611]' rad/s, and k_p=1

2.2 Modifying Slider Mass While Increasing k_p

Changing the mass of each slider dictates changes to the configuration of the system and requires different linear actuators. Applying these considerations, each sliding mass increases to 50 kg and k_p=1000 producing the following results.

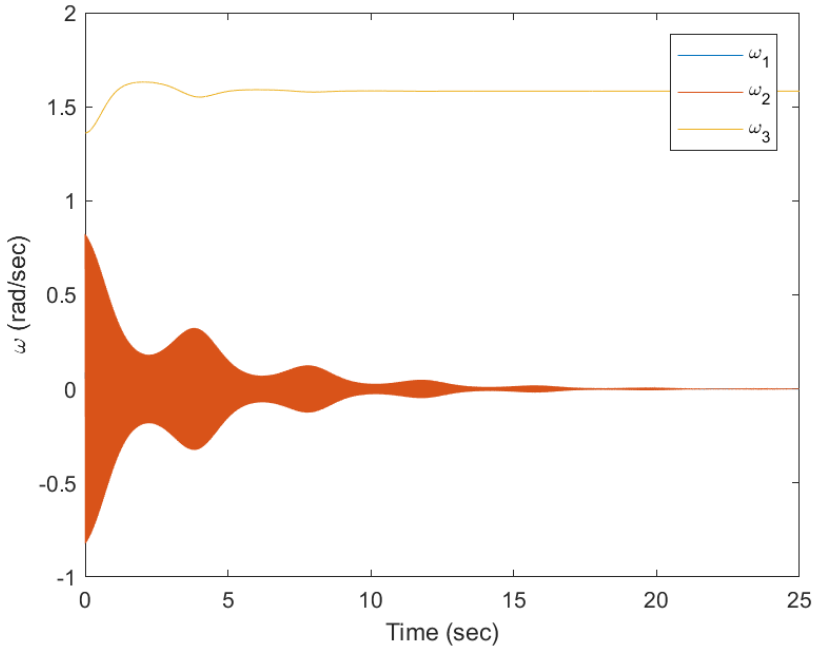

Figure 37. Angular Velocity (rad/s) with a simulator mass of 1375 kg, slider mass of 50 kg, MOI=diag(1100; 2100; 1050) kg m^2, ω_0=[0.0888 0.8229 1.3611]' rad/s, and k_p=1000

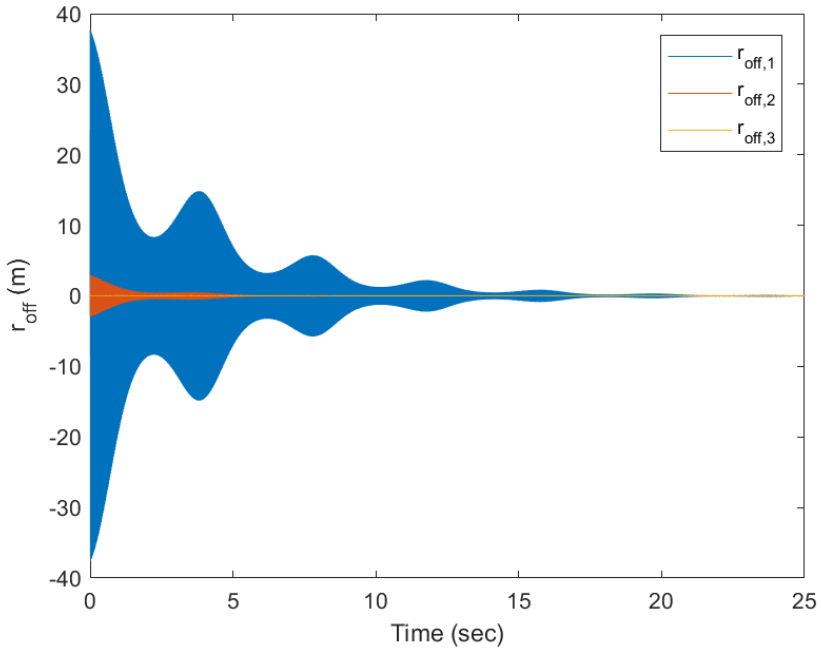

Figure 38. Determination of r_{off} with a simulator mass of 1375 kg, slider mass of 50 kg, MOI=diag(1100; 2100; 1050) kg m^2, ω_0=[0.0888 0.8229 1.3611]' rad/s, and k_p=1000

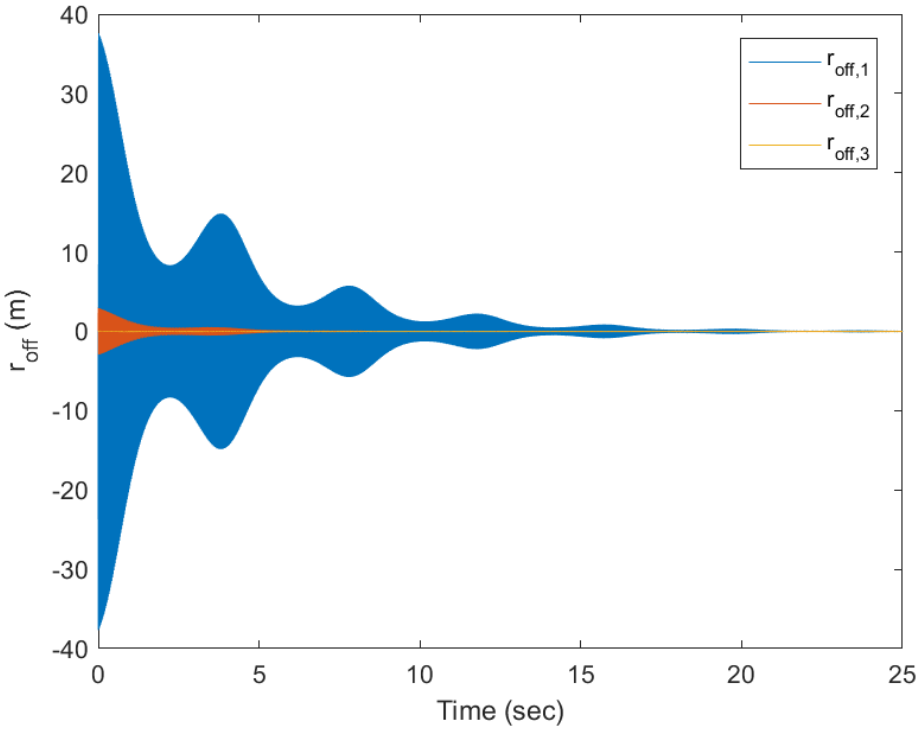

Figure 39. Estimated offset error of COM displacement with a simulator mass of 1375 kg, slider mass of 50 kg, MOI=diag(1100; 2100; 1050) kg m^2, ω_0=[0.0888 0.8229 1.3611]' rad/s, and k_p=1000

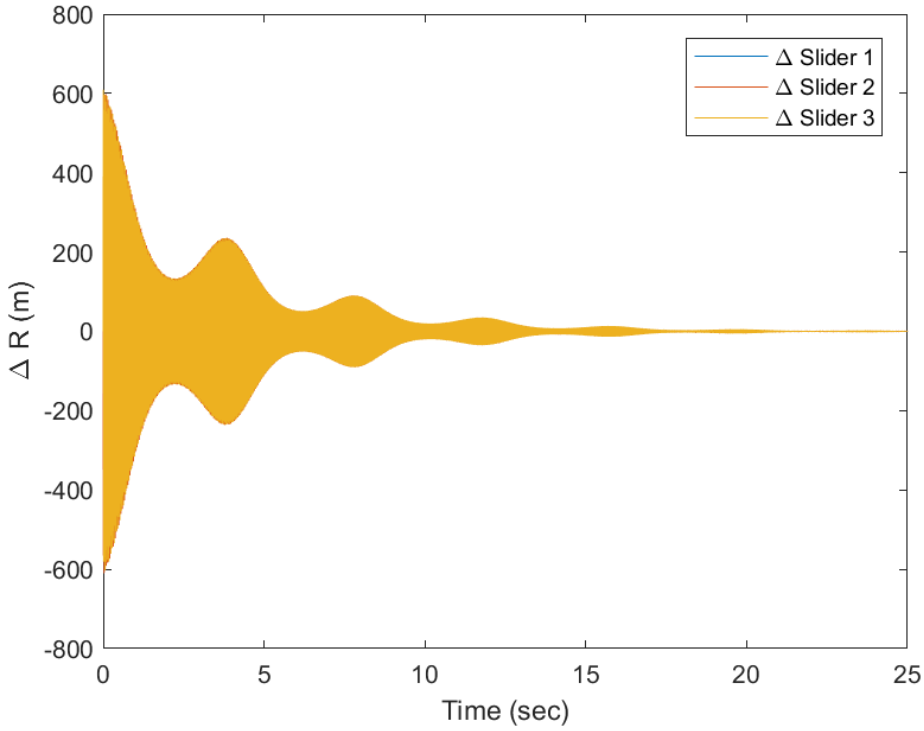

Figure 40. Change in horizontal slider positions with a simulator mass of 1375 kg, slider mass of 50 kg, MOI=diag(1100; 2100; 1050) kg m^2, ω_0=[0.0888 0.8229 1.3611]' rad/s, and k_p=1000

This simulation converges at a much more reasonable rate; however, the travel of the sliding masses is still impractical. This change substantially reduces the distance each slider travels. However, having the masses travel 1.2 km is highly impractical. To fully realize an acceptable solution requires refining the tuning of k_p.

Bibliography

[1] Y. Liu, L. Li, Z. Fu, J. Tan, and K. Li, "Automatic mass balancing of a spacecraft simulator based on non-orthogonal structure," in *2016 UKACC International Conference on Control*, 2016.

[2] D. Penn, *Characterization and Modeling of a Control Moment Gyroscope*. Masters thesis, Air Force Institute of Technology, 2015.

[3] M. Garcia, "NASA Astronauts Go Underwater to Test Tools for a Mission to an Asteroid." `https://www.nasa.gov/content/nasa-astronauts-go-underwater-to-test-tools-for-a-mission-to-an-asteroid`, 2014.

[4] J. L. Schwartz, M. A. Peck, and C. D. Hall, "Historical Review of Air-Bearing Spacecraft Simulators," *Journal of Guidance, Control, and Dynamics*, vol. 26, no. 4, pp. 513–522, 2003.

[5] H. Schaub and J. L. Junkins, "Singularity Avoidance Using Null Motion and Variable-Speed Control Moment Gyros," *Journal of Guidance, Control, and Dynamics*, vol. 23, no. 1, pp. 11–16, 2000.

[6] J. J. Kim and B. N. Agrawal, "Automatic Mass Balancing of Air-Bearing-Based Three-Axis Rotational Spacecraft Simulator," *Journal of Guidance, Control, and Dynamics*, vol. 32, no. 3, pp. 1005–1017, 2009.

[7] S. Chesi, Q. Gong, V. Pellegrini, R. Cristi, and M. Romano, "Automatic Mass Balancing of a Spacecraft Three-Axis Simulator: Analysis and Experimentation," *Journal of Guidance, Control, and Dynamics*, vol. 37, no. 1, pp. 197–206, 2014.

[8] B. L. Reifler and D. R. Penn, "Integration of a Motion Capture System into a Spacecraft Simulator for Real-Time Attitude Control," Tech. Rep., Air Force Research Lab, Kirtland AFB, Kirtland AFB, NM, 2016.

[9] Z. Xu, N. Qi, and Y. Chen, "Parameter estimation of a three-axis spacecraft simulator using recursive least-squares approach with tracking differentiator and Extended Kalman Filter," *Acta Astronautica*, vol. 117, pp. 254–262, 2015.

[10] "Definition of FRICTION." `https://www.merriam-webster.com/dictionary/friction`, 2018.

[11] A. Das, J. Berg, G. Norris, D. Cossey, T. J. Strange, and W. Schlaegel, "ASTREX - A Unique Testbed for CSI," in *Decision and Control, 1990., Proceedings of the 29th IEEE Conference on Decision and Control*, (Honolulu, HI), pp. 2018–2023, IEEE, 1990.

[12] J. E. Colebank, R. D. Jones, R. D. Pollak, D. R. Mannebach, and G. R. Nagy, "SIMSAT: A Satellite System Simulator and Experimental Test Bed for Air Force Research," Masters Thesis, Air Force Institute of Technology, 1999.

[13] G. A. Smith, "Dynamic Simulators for Test of Space Vehicle Attitude Control Systems," in *Proceedings of the Conference on the Role of Simulation in Space Tecnology, Part C*, (Blacksburg, VA), pp. XV–1 TO XV–30, 1964.

[14] C. E. Skelton II, "Mixed Control Moment Gyro and Momentum Wheel Attitude Control Strategies," Masters Thesis, Virginia Polytechnic Institute and State University, 2003.

[15] R. H. Kraft, "CMG Singularity Avoidance in Attitude Control of a Flexible Spacecraft," *Proc. Am. Control Conf.*, no. 6, pp. 56–58, 1993.

[16] S. Chesi, Q. Gong, and M. Romano, "Aerodynamic Three-Axis Attitude Stabilization of a Spacecraft by Center-of-Mass Shifting," *Journal of Guidance, Control, and Dynamics*, vol. 40, no. 7, pp. 1–14, 2017.

[17] W. Yan, H. Cheng, and C. X. Lin, "Automatic mass balancing and design of a six degrees-of-freedom air bearing spacecraft simulator," in *Chinese Control Conference, CCC*, vol. 2015-Septe, pp. 5696–5700, 2015.

[18] F. L. Markley and J. L. Crassidis, *Fundamentals of Spacecraft Attitude Determination and Control*. New York: Springer, 2014.

[19] K. W. Johnson, "Intermediate Space Flight Dynamics, Part 24-25: Linear control theory and stability," Course Notes, 2017.

[20] S. J. Julier and J. K. Uhlmann, "New extension of the Kalman filter to nonlinear systems," *Int. Symp. Aerospace Defense Sensing Simul. and Controls*, vol. 3, p. 182, 1997.

[21] P. Sekhavat, Q. Gong, and I. M. Ross, "NPSAT1 Parameter Estimation Using Unscented Kalman Filtering," *Proc. IEEE American Control Conf.*, pp. 4445–4451, 2007.